THESIS FOR THE DEGREE OF DOCTOR OF PHILOSOPHY

Analysis of Carbon Black Oxidation

Experimental Methods, Kinetic Study, and Model Development

SOHEIL SOLTANI

CHALMERS

Department of Chemistry and Chemical Engineering
Chalmers University of Technology
Gothenburg, Sweden, 2017

Analysis of Carbon Black Oxidation

Experimental Methods, Kinetic Study, and Model Development

SOHEIL SOLTANI

ISBN 978-91-7597-564-1

Doktorsavhandlingar vid Chalmers tekniska högskola,
Ny serie nr. 4245
ISSN 0346-718X

Department of Chemistry and Chemical Engineering
Chalmers University of Technology
SE-412 96 Gothenburg, Sweden
Telephone: +46 (0)31-772 10 00

Cover: Mount Damavand dimmed under a dense layer of pollutants with the $PM_{2.5}$ index reaching above 150 (left) compared with a clean day (right). Particulate matter, carbon monoxide, and nitrogen oxides continue to be the most severe sources of air pollution in Tehran and similar cities. Even though the technology is mature enough to substantially reduce these emissions, the need for implementation remains to be understood and prioritized. Photos from www.ifpnews.com and www.bestbist.com.

Chalmers Reproservice
Gothenburg, Sweden (2017)

Analysis of Carbon Black Oxidation

Experimental methods, Kinetic Study, and Model Development

Soheil Soltani
Department of Chemistry and Chemical Engineering
Chalmers University of Technology, Gothenburg, Sweden

Abstract

Diesel engines are known to be a major source of a highly pollutant material known as particulate matter, PM, which is a strongly threatening agent to human health. Therefore, diesel particulate filters are used to reduce PM emissions by trapping soot. Regenerating the particulate filter is necessary to keep the exhaust back pressure below a certain limit and, thereby, to maintain efficient fuel consumption. Regeneration can be run in two modes: active or passive. The former mode is performed by injecting additional fuel into the exhaust to raise the temperature above 550 ^{o}C and, thereby, burn the accumulated soot with oxygen. In contrast, passive regeneration can be performed at the exhaust temperature, i.e. 350-450 ^{o}C, which is more efficient. The key compound for passive regeneration that reacts with soot is NO_2, which is more reactive than oxygen. It is formed by oxidizing NO over an oxidation catalyst.

The goal of this thesis is to develop both experimental and theoretical methodologies to study the soot-NO_2 reaction from a fundamental perspective. To this end, a thorough characterization study of the experimental setup was conducted with respect to heat transfer and residence time distribution, which resulted in a number of guidelines to help increase the quality of experimental measurements. Moreover, a novel sample preparation method is proposed that ensures a highly controlled carbon deposition in each and every channel of the monolithic reactors, which was found to be crucial for obtaining reliable and reproducible results. Furthermore, a deconvolution algorithm was developed to decrease the unresolved time span of transient measurements. Numerical simulations, in particular computational fluid dynamics, were extensively employed to both aid as simulation tools and to gain a deeper insight into the subject of study.

Significant promoting effects were identified for both water vapor and molecular oxygen, which indicates the importance of studying automotive soot oxidation under realistic exhaust conditions. A global kinetic model was formulated that can express the observed rate of oxidation in the presence of water vapor, oxygen, and NO_2 with very high accuracy over the entire 0-100% conversion interval. It thus serves as a predictive tool for optimizing both the operation of diesel engines and the design of soot traps.

Keywords: diesel particulate filter (DPF), computational fluid dynamics (CFD), transient kinetics, inverse problems, deconvolution, kinetic modeling, residence time distribution

In memory of
Dr. Hossein Fatemi
and Dr. Mohammad Mosaddegh

List of Appended Papers

This thesis is based on the work reported in the following papers, referred to by Roman numerals in the text:

Paper I

Kinetic Analysis of O_2- and NO_2-based Oxidation of Synthetic Soot
Carolin Wang-Hansen, Soheil Soltani and Bengt Andersson
Journal of Physical Chemistry C, 117 (2013) 522–531

Paper II

CFD Characterization of Monolithic Reactors for Kinetic Studies
Soheil Soltani, Carolin Wang-Hansen, Ronnie Andersson and Bengt Andersson
Canadian Journal of Chemical Engineering, 92 (2014) 1570–1578

Paper III

Time Resolution in Transient Kinetics
Soheil Soltani, Ronnie Andersson and Bengt Andersson
in: Beilina L. (Ed.) Inverse Problems and Application, Springer (2015) 81–96

Paper IV

Enhancement of Time Resolution in Transient Kinetics
Soheil Soltani, Ronnie Andersson, Bengt Andersson
Chemical Engineering Journal, 264 (2015) 188–196

Paper V

Oxidation of synthetic soot with NO_2 in the presence of water vapor and oxygen
Soheil Soltani, Ronnie Andersson, Bengt Andersson
Submitted to Carbon

Related publications not included in this thesis:

Gas Phase Residence Time Distribution in Closed Crossed-Flow Structured Packings for Multiphase Co-current Downflow Tubular Reactors
David Vervloet, Soheil Soltani, Freek Kapteijn, John Nijenhuis, J. Ruud van Ommen

In manuscript

Author's contribution to the publications:

Paper I

I formulated the population balance model and simulated it. The results were analyzed together with the co-authors.

Paper II

I conducted the experiments with the laboratory reactor setup, developed the CFD model, performed the simulations, and developed the deconvolution algorithm. I wrote and submitted the manuscript. The results were interpreted together with my co-authors.

Paper III

I conducted the experiments, formulated the mathematical problem, elaborated the details of the deconvolution algorithm, developed and released the Open Source software package. I wrote and submitted the manuscript. The results were analyzed together with my co-authors.

Paper IV

I developed the CFD model, implemented its computational subroutine in a user-defined function (UDF), and performed the simulations. I wrote and submitted the manuscript. The results were analyzed together with my co-authors.

Paper V

I conducted the experiments, proposed and tested the new sample preparation method, conceived and conducted the temperature-programmed desorption experiment to investigate the influence of surface oxygen complexes. I developed the kinetic model and implemented it in a computational model, performed the population balance analysis, and wrote the manuscript. The results were interpreted together with my co-authors.

List of acronyms

ASA	active surface area
BP	basal plane
CFD	computational fluid dynamics
cpsi	cells per square inch
CSTR	continuous stirred tank reactor
DO	discrete ordinates
DPF	diesel particulate filter
DRIFTS	diffuse-reflectance Fourier-transform spectroscopy
FTIR	Fourier-transform infra-red
HRTEM	high-resolution transmission electron microscope
IR	infra-red
MEX	Matlab EXecutable
MS	mass spectroscopy
ODE	ordinary differential equation
PM	particulate matter
RSA	reactive surface area
RTD	residence time distribution
TPD	temperature-programmed desorption
TSA	total surface area
URSA	unreactive surface area

Contents

1

Introduction

1.1 Particulate matter

Diesel particulate filters (DPFs) have been developed for efficient particulate matter mitigation in the exhaust after-treatment of diesel engines. In order to maintain an acceptable exhaust back-pressure (typically 150 mbar), regeneration is necessary to burn the accumulated soot off the filter. NO_2 is an important component of the exhaust that is very reactive towards soot oxidation. The reactivity of NO_2 towards soot oxidation is higher than that of other oxidants, such as N_2O, NO, and O_2 [1]. Furthermore, it can oxidize the carbonaceous matter in the soot cake at exhaust temperature, i.e. 350-450 °C, and, therefore, it plays a central role in the passive regeneration of DPFs. Subsequently, the fuel penalty paid for active regeneration at elevated temperatures can be alleviated, or substantially reduced, along with a reduced risk of melting the filter due to a runaway reaction. NO_2 is formed upstream of a DPF in the diesel oxidation catalyst by oxidizing NO. A DPF coated with platinum (Pt) is also capable of oxidizing NO to NO_2.

The terms soot and particulate matter (PM) are often used interchangeably, and they both refer to the fine particles that are present in the exhaust of combustion processes. PM is known to be a severely pollutant material, and it has been proven to have carcinogenic effects [2]. PM also poses a prime health threat to people with respiratory and cardiovascular diseases [3, 4]. It is estimated that $PM_{2.5}$, i.e. fine particles smaller than 2.5 μm, is responsible for around 3 million annual pre-mature mortalities worldwide [5]. Diesel engines are the major contributors to $PM_{2.5}$, and, consequently, DPFs play a critical role by reducing these emissions.

1. INTRODUCTION

In terms of chemical and physical properties, particulate matter is not a well-defined material. The solid fraction of PM is mainly comprised of carbonaceous matter and ash, the latter of which mainly originates from lubricating oil. There are also detectable amounts of condensed hydrocarbons, sulfuric acid, and water adsorbed on soot, which form the liquid fraction of PM [3]. Soot is formed during the course of fuel combustion in an engine. At this stage, it is mainly made up of the so-called primary particles that span a size range of a few nm up to 10-20 nm. These particles are more or less spherical and sticky. Due to agglomeration and interactions with the walls of the after-treatment system, micron-sized aggregates of PM are formed that are no longer as spherical as the primary particles. These are known as coarse-mode particles [3].

High-resolution, transmission electron microscope (HRTEM) images of PM reveal more structural details. In general, a significant degree of aggregation between primary particles has been observed at low magnification [6]. Figure 1 shows the nanostructure of a soot sample obtained from the filter of an on-road heavy-duty diesel engine. The periphery of the particles is moderately graphitic, and the interior lamellae are somewhat tortuous and randomly oriented [6].

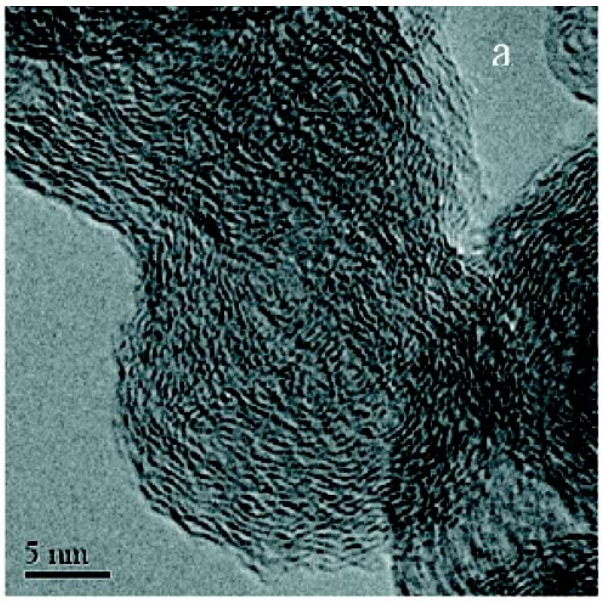

Figure 1: HRTEM image of soot from the filter of a heavy-duty diesel engine [6].

The carbonaceous lamellae of soot are composed of graphitic layers in which individual carbon atoms are located either on the edge plane or on the basal plane, as illustrated

in Figure 2. Carbon sites on the edge plane exist in two different configurations, namely zigzag and armchair sites, on which different oxygen complexes are preferentially formed [7, 8, 9].

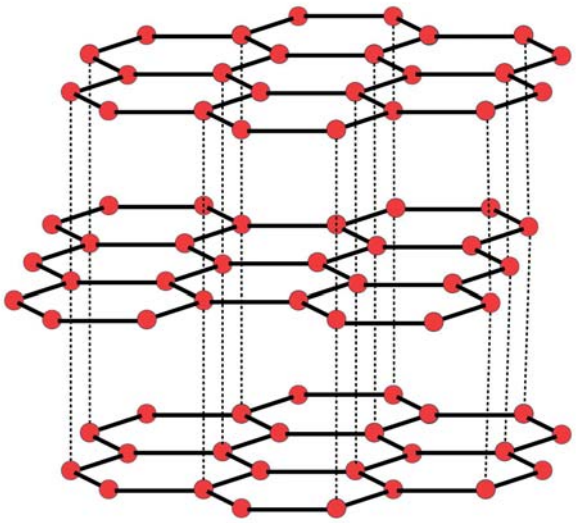

Figure 2: Carbon sites on the edge and basal planes constituting a graphitic structure.

Graphitization is both a thermally- and oxidative-induced process during which the carbonaceous lamellae undergo reorientation to form more ordered and energetically more stable configurations. By this means, the ratio of the edge to basal plane sites, and, thereby, the overall reactivity of the carbonaceous matter decreases. Graphitization through thermal processes occurs due to the desorption of volatile compounds as well as the carbonization of adsorbed hydrocarbons, which results in the formation of active sites for enhancing the growth of carbon lamellae. Elevated temperatures also provide the required energy for reorientation [10].

Oxidation preferentially removes the amorphous fraction of carbon, which leads to a more graphitic structure. As a result, porosity, and, thereby, the overall surface area increases until a critical point is reached at which the carbon structure collapses. This causes a substantial loss of the accessible surface area, which in turn decreases the observed reactivity [10].

HRTEM images have also revealed evidence of graphitization and the consequent loss of reactivity during progressive oxidation [10]. Figure 3 shows an HRTEM image of a soot sample collected from the filter of an urban bus that had been running for a prolonged period of weeks. Several core-shell structures consisting of hollow interiors (shown by arrows) and graphitized shells were observed [10].

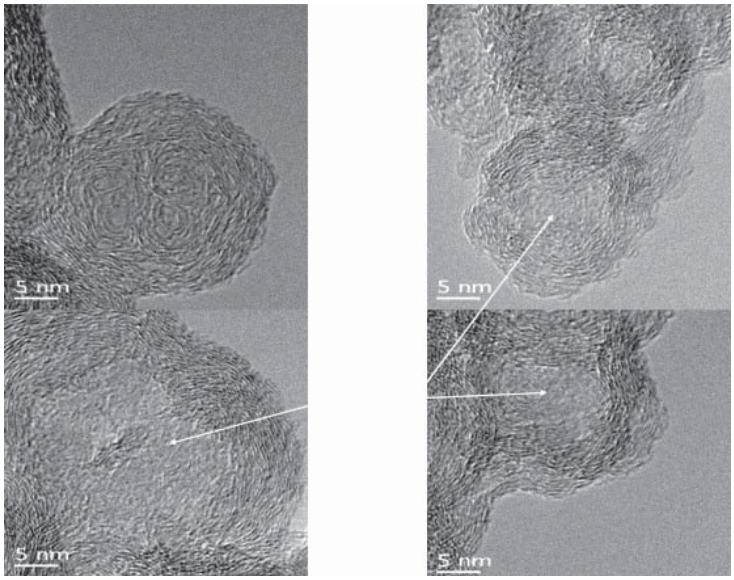

Figure 3: Internal oxidation of soot, which forms hollow shells [10].

Some differences were observed for two other soot samples collected during 10-12 hours and at different engine loads. The soot sample that was collected during a fairly high engine load exhibited both uniform particles and hollow shells, while the one collected at a fairly low load consisted mainly of uniform particles. However, the development of the hollow structures with graphitized shells was observed in the latter sample upon partial oxidation at 450 °C to about 1/2 of the initial mass, as depicted in Figure 4.

Interestingly, Printex-U samples did not show such a transformation, and, therefore, it was concluded that the origin of the primary particles likely played a role in the evolution of the carbon nanostructure [10].

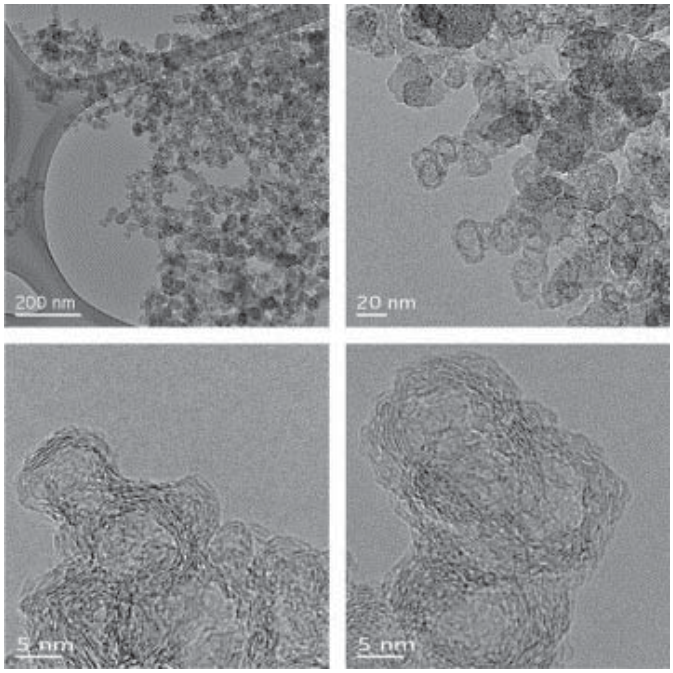

Figure 4: Formation of hollow particles after partial oxidation [10].

1.2 Objectives of the study

The central objective of this research was to study non-catalytic oxidation of carbonaceous matter at low to moderate temperatures pertinent to the passive regeneration of DPFs. As discussed earlier, carbon-NO_2 reaction would consequently be the most relevant reaction to investigate. Hereinafter, carbon oxidation will refer to this particular reaction unless otherwise specified. A substantial part of this study was conducted experimentally; therefore, the characterization of the reactor setup was deemed necessary to obtain reliable measurements. The following reactions have been proposed to summarize the elementary steps comprising carbon combustion with NO_2 [1]:

$$2NO_2 + C \rightarrow 2NO + CO_2 \tag{1}$$

$$NO_2 + C \rightarrow NO + CO \tag{2}$$

It was deemed necessary to elaborate more on the underlying mechanisms of these reactions, in particular to clarify whether the combustion products are formed through a single or parallel mechanism. Therefore, transient kinetic methods were employed to reveal the mechanistic information of the reaction. However, substantial signal distortion was observed in concentration measurements. Therefore, the residence time distribution

(RTD) in the reactor setup, and, in the gas cell of the detector, in particular, was studied in detail. Consequently, a mathematical algorithm for deconvolution was developed that decreased the unresolved time interval of transient measurements. Alternatively, it was shown that deconvolution can be used to reconstruct unknown RTDs from the results of step- or pulse-response experiments. Furthermore, compounds with non-linear IR absorption will be demonstrated as the source of a systematic error that affects the transient periods of FTIR-based concentration measurements.

The influence of water vapor and molecular oxygen as important components of diesel exhaust that exert a substantial promoting effect on the rate of carbon oxidation with NO_2 was investigated experimentally. Moreover, a methodology for formulating kinetic models of soot oxidation under realistic exhaust conditions was developed.

1.3 Thesis outline

The reactor setup as well as the experimental procedure used in this study will be described first, and a new method for sample preparation will be introduced. A theoretical study will follow, which starts by expressing the need for the characterization of the experimental equipment and continues with the mathematical aspects of the deconvolution algorithm. The aim is to demonstrate the importance of such fundamental aspects in connection with a successful, reliable, and physically-sound kinetic study. Next, carbon oxidation, in general, and with NO_2 in particular, will be discussed with an emphasis on the promoting effect of water vapor and molecular oxygen on this reaction. Surface oxygen complexes and the role of the mobility of chemisorbed oxygen will be briefly reflected on. The results of this study are given in Section 5 followed by the conclusions and outlook of the thesis for future research.

2

Experimental Studies

The experimental setup consisted of a flow-reactor system with monolithic substrates. The main components of the setup were mass-flow controllers, a quartz tube that confined the monolithic modules and thermocouples, pre-heaters and a heating coil, insulation material, and finally a Fourier transform infra-red (FTIR) gas analyzer. Temperature was measured using K-type thermocouples. One thermocouple was placed in an inert substrate in the upstream of the reactor to control the temperature of the gas phase. A second thermocouple was placed in the rear part of a reactor channel to monitor the reaction temperature. This thermocouple was chosen to be slightly thicker to ensure a good contact between the solid walls of the reactor and the thermocouple. Figure 5 shows a schematic layout of the setup. More information can be found in the detailed characterization study that was performed [11].

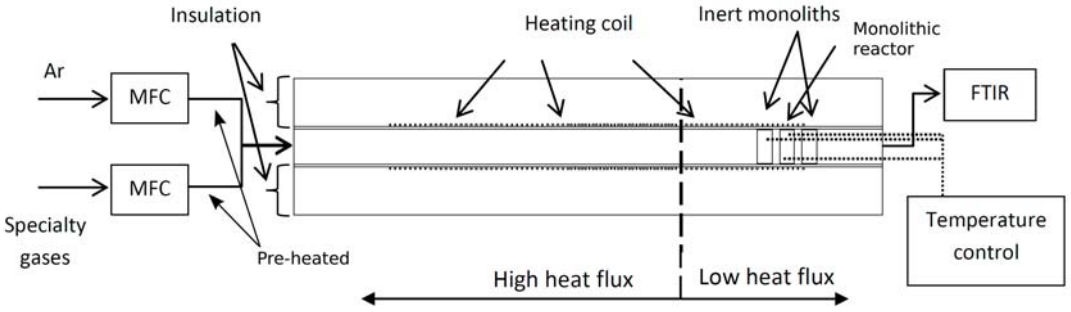

Figure 5: Schematic layout of the reactor setup [11].

2.1 Sample preparation

Monolithic modules consisting of 188 channels (400/4 cpsi) with a length of 20 mm and a diameter of 22 mm were used as the substrate for sample preparation. The samples were prepared using Printex-U as a surrogate for diesel soot with well-defined properties. The reason for this was to obtain reproducible results that could lead to establishing the test methodologies. Once this goal was fulfilled, the methods could be applied to real soot samples.

At first, the preparation method used in the earlier studies of our research group was adopted, which is the dry-shaking of a bare monolith in a plastic container with approx. 5 mL Printex-U [12]. However, due to the more stringent requirements of the studies of passive regeneration at substantially lower temperatures, two major problems with this method were diagnosed. First, as reported in the previous study, the achievable loading with this method that can result in a rather uniform carbon deposition is limited to a few milligrams. Despite being above the detection limit, the concentration of the oxidation products at such a low loading and at 350 °C was too low to obtain an appropriate signal-to-noise ratio. Second, although the preparation method was reported to produce uniform samples, at even low loadings of around 6 mg it could be seen that more carbon was deposited on the two ends of the substrate where the maximum impulsive force due to shaking was exerted (cf. Figure 1A in [12]). This issue becomes much more pronounced if more powder is used for sample preparation in order to achieve higher loadings. Additionally, if the loosely-bound carbon is not removed from the sample prior to an experiment, there will be a risk of having it blown out and carried over to other regions of the reactor setup. Due to poor control over the distribution of carbon among and within the reactor channels, there is a risk of depositing too much powder in some channels than in others. In fact this was found to lead to unphysical observations such that a lower reaction rate would be measured despite a higher temperature and/or a higher concentration of NO_2 as illustrated in Figure 6. Additionally, the reproducibility of the results was found to be very poor, as shown in Figure 7, for a number of replicated experiments at 400 °C with 400 ppm NO_2 and 5% water in the inlet.

A new method that yields more precise control over powder distribution and loading was, therefore, proposed and used in the present study. This method helps achieve a more uniform carbon deposition even at loadings of approx. 15 mg. In this method, a thin brush dipped into dry, powdered Printex-U is inserted into each and every channel from

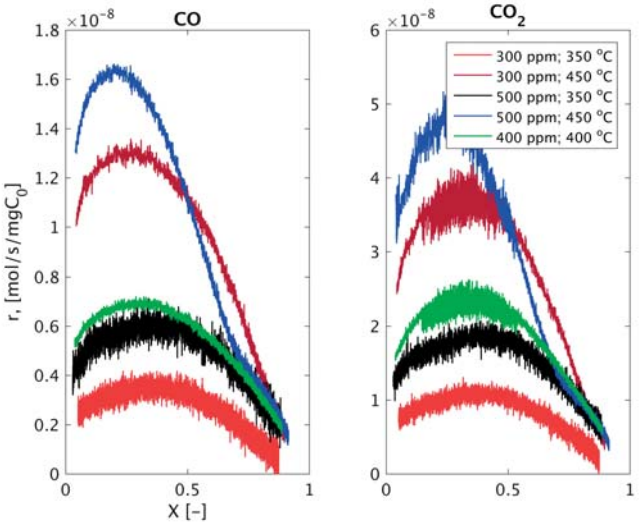

Figure 6: Unreliable results obtained using samples of poor quality.

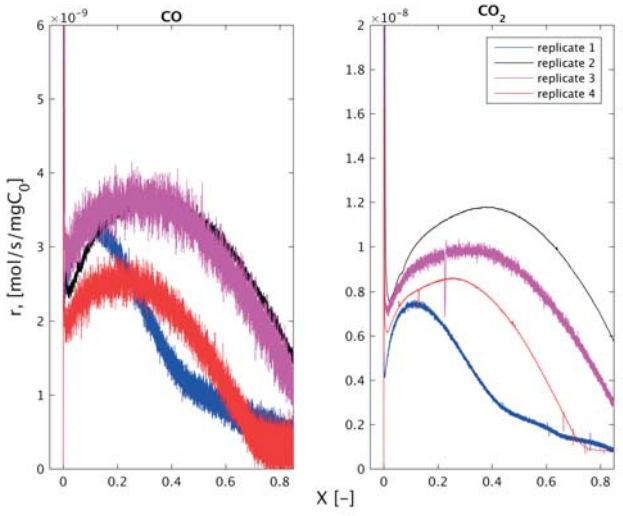

Figure 7: Failures to obtain reproducible results due to the variable quality of the samples.

both ends while the brush is slightly rotated at the same time. The excess of the powder was subsequently removed with a mild impact force, e.g. knocking on a lab workbench, as well as using a moderate flow of air through the monolith channels. This was done to prevent the loosely bound soot from being blown out of the reactor during the course of an experiment, in which case it would reside in the outlet region of the setup and would give rise to erroneous measurements.

The alternative method of preparing samples was found to have a tremendous effect on obtaining both physically sound and reproducible results as depicted in Figures 8 and 9. It is worth mentioning that the reproducible results shown in Figure 9 were obtained for experiments conducted at one of the most challenging conditions with respect to temperature and inlet concentration of NO_2, i.e. 450 °C with 300 ppm NO_2 in the presence of 5% water.

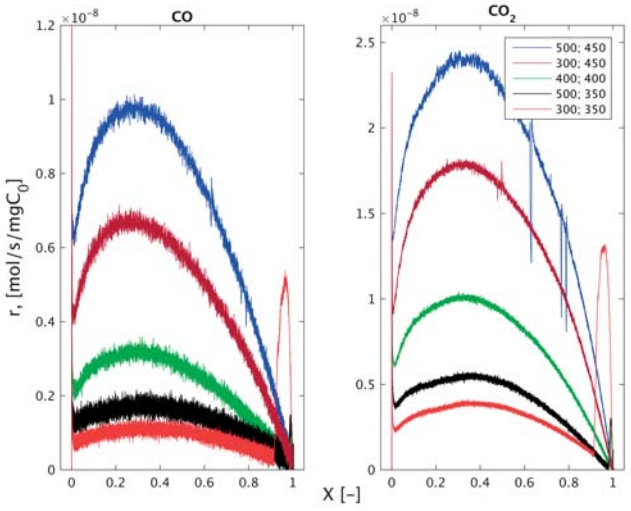

Figure 8: Improved quality and theoretical consistency of the experimental results as a consequence of the improved quality of the samples.

The monoliths were weighted three times: once before deposition; once after deposition; and once after the oxidation experiments. The difference between the first and the second measurements gives an indication of the amount of deposited carbon, which was typically close to but not precisely equal to the difference between the last two measurements. This was mainly due to channel breakage at the time of (un)mounting the samples because of the tight contact between the channel walls and the thermocouple. Typical

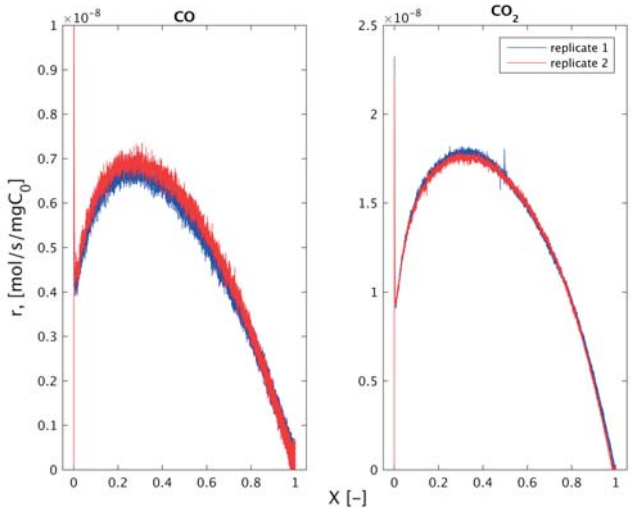

Figure 9: Largely reproducible results obtained through controlled carbon deposition.

loadings achieved with this method were between 10-15 mg.

2.2 Experimental procedure

The two main experimental plans that were used in this study were step-response experiments and steady-state oxidation in the presence of water and oxygen. Each routine will be further described in this section. In all the experiments, a sample was heated up to 600 °C under an inert flow of argon in order to degas the surface. After the pre-treatment step, the temperature was reduced to the target point, and the experiments were commenced after a constant temperature had prevailed. The experiments were eventually terminated by oxidizing the remaining carbon at an elevated temperature of 600 °C for 1-2 hour(s) to allow the carbon balance to close. The initial mass of carbon was calculated by integrating the concentration of CO and CO_2 with respect to time. The result of this is fairly comparable with the result obtained by weighting the sample, as described before.

2.2.1 Step-response experiments

This experimental routine consisted of step changes to 500 ppm NO_2 for 2 minutes followed by a relaxation period that lasted for 3 minutes in which the gas phase composition

was rapidly switched to inert. The main focus of this routine was on the decaying profile of the oxidation products.

2.2.2 Isothermal oxidation in the presence of water vapor and oxygen

A set of isothermal experiments was designed, and the experiments were conducted with four effects: i) concentration of NO_2 (300-500 ppm); ii) concentration of water (0-5 vol. %); iii) concentration of O_2 (0-3 vol. %); and iv) temperature (350-450 ^{o}C). The duration of each experiment was typically 3-5 hours before the temperature ramp started.

3

Characterization of the Experimental Setup

Oxidation of carbonaceous matter in a diesel particulate filter (DPF) or even in a laboratory reactor constitutes a multi-scale system with different processes that occur over a broad range of scales, from the reactor scale to the atomistic scale where the reactions occur. Therefore, a great deal of fundamental studies is required to gain a deeper understanding of each part of the system. This thesis reflects some of these fundamental aspects; including the characterization of the reactor setup, extending the boundaries of transient kinetic methods using numerical techniques, and acquiring kinetic information on the reaction.

3.1 Analysis of heat transfer and residence time distribution

Carbon oxidation is a heterogeneous exothermic reaction, and, therefore, obtaining reproducible and reliable kinetic data from experimental studies requires special consideration of the interplay between transport phenomena and kinetics. The established temperature profile inside a reactor is a crucial parameter in particular. Ideally, an isothermal operating condition is desirable for kinetic analysis. This was the central point of Paper II, which aimed at improving the quality of experimental measurements by means of a detailed analysis of flow, temperature, and concentration distributions throughout the reactor setup [11]. A two-dimensional, axisymmetric CFD model was developed that included radiative heat transfer as a significant mechanism of energy transport.

3. CHARACTERIZATION OF THE EXPERIMENTAL SETUP

An earlier study in our research group had found experimental evidence of the significance of radiation shielding for obtaining a more uniform temperature distribution inside a monolithic reactor [12]. Examining the role of radiative heat transfer was, therefore, of central interest in the present study, and was implemented in the CFD model of the setup using the method of discrete ordinates (DO). This model is suitable for simulating radiation through participating media, and a detailed description of the model can be found elsewhere [13].

Additionally, the error in temperature measurements resulting from thermal radiation to an unshielded thermocouple was investigated using the surface-to-surface radiation model. This model consists of the calculation of view factors and is suitable for simulating radiative heat transfer in an enclosure of surfaces.

Furthermore, the different parts of the setup were individually characterized with respect to hydrodynamic dispersion, which is of particular importance for analyzing transient experiments (cf. Section 5.2 for further details).

A solution was proposed to compensate for the loss in temporal resolution using deconvolution of transient data, and an Open Source algorithm was developed accordingly. The official repository of the software contains the algorithm and its documentation [14].

Deconvolution is an inverse problem that has ill-posed characteristics in the presence of experimental noise. A thorough description of the theoretical background of this particular problem is given in Paper III, which shows that the developed algorithm can successfully handle the noise in experimental data [15].

It was also shown that a systematic error affects transient measurements involving species with non-linear infra-red absorption arising from a non-homogeneous concentration distribution. This was touched on in Paper II, and an additional analysis is given in Paper IV. The analysis of deconvolution was also extended in Paper IV by studying the effects of mean residence time in the gas cell of an FTIR analyzer and the sampling frequency of its detector.

3.2 Ill-posedness of a deconvolution problem

The enhancement of temporal resolution consists of an ill-posed problem, which requires special considerations. According to Hadamard, a well-posed problem satisfies the following conditions [16, 17]:

1. The existence of a solution
2. The uniqueness of the solution
3. The solution is a continuous function of the initial data.

If any of these are violated, the problem is said to be ill-posed.

The second and the third conditions above are of great importance for deconvolution problems. These problems are mathematically described by the Fredholm integral equation of the first kind, for which it can be shown that the presence of arbitrarily small perturbations in the measured data results in arbitrarily large oscillations in the reconstructed solution [18]. This clearly indicates that the third condition is violated, and that the uniqueness of the solution is not guaranteed because solutions with a varying extent of stability may satisfy the forward problem.

Consequently, the solution to ill-posed, inverse problems requires an additional condition of smoothness, and this method of stabilizing the solution is known as regularization. A widely used regularization method for linear ill-posed problems has been introduced by Tikhonov, and this is the one that was implemented in our deconvolution algorithm [19].

Of central importance to Tikhonov's regularization method is the calculation of the regularization parameter. To this end, attempts were made initially to use rather simple methods like the Hansen L-curve method [18]. However, the results in the best case were identical to those of the theoretically sound method of the discrepancy principle, which is the only method that accounts for the uncertainties that are originally present in measured data [20]. Convergence of the other, so-called error-free methods are questionable [21], therefore, the discrepancy principle was implemented in the software. This means that the accuracy of the reconstructed solution must be in accordance with that of the original data.

3.3 Non-linear IR absorption and FTIR spectroscopy in transient experiments

It was found that a non-homogeneous concentration profile pertains throughout the gas cell of an FTIR analyzer during transient periods [11]. This results in a systematic error if the species being measured exhibits a non-linear absorption-concentration relationship. That is because measuring the concentration of species with non-linear IR absorption is dependent on the concentration distribution within the gas cell and cannot be approximated by an average concentration within the cell. A detailed study of this systematic error was conducted in Paper IV using a 3-dimensional CFD model of a gas cell. The Beer-Lambert law was implemented in the model through a user-defined function [22]. The simulations consisted of carbon monoxide and nitric oxide, which are known to have non-linear IR absorption. The results clearly showed a systematic deviation in the measured concentration during a transient period, which was understood to be dependent on the concentration at the inlet. Consequently, the error was not possible to be compensated for with a simple calibration-like correlation. Therefore, a compartment model for the gas cell was proposed that includes the results of the CFD simulations in a lookup table that can be used to correct the systematic error.

4

Analysis of Carbon Oxidation

4.1 Surface oxygen complexes

Oxygen-containing complexes on a carbonaceous surface span a broad range of chemical structure and thermal stability [23]. Oxygenated complexes that are formed upon the interaction between NO_2 and carbon are of particular relevance for this study. Therefore, the results of a DRIFTS study conducted by Muckenhuber and Grothe on carbon-NO_2 interaction, in particular with Printex-U, are briefly reviewed here [23].

Subsequent to carbon-NO_2 interaction at room temperature, only one absorption band was observed at 1220 cm^{-1}, which was also observed at 400 °C but with much more intensity. This band is assigned to the vibration of the C-O bond in C-ONO. After the reaction at 400 °C, several other bands were observed as well, which were assigned to their corresponding functional groups as in Table 1. The absorption band at 1785 cm^{-1} was attributed to the formation of carboxylic anhydrides, which are formed as a result of the oxidation of pre-existing oxygenated groups. This reaction does not occur on degassed surfaces.

Subsequently, the sample was stepwise heated to different temperatures up to 300 °C, and after each step, a spectra was recorded at room temperature. It was found that the chelated bond between NO_2 and carbon is less stable than the non-chelated bond because the former disappears first. More importantly, it was observed that with heat treatment to 300 °C, two new bands appeared at 1565 and 1400 cm^{-1}. These were concluded to be due the formation of an acidic functional group as C(=O)ONO, which is only an intermediate because no absorption band at 1730 cm^{-1}, i.e. the characteristic of a carboxylic

group, was observed. This intermediate decomposed as NO and C(=O)O, the latter of which may then desorb as CO_2.

The formation of an acidic complex as an intermediate was previously observed in an earlier study by Muckenhuber and Grothe in which temperature-programmed desorption-mass spectroscopy (TPD-MS) was combined with DRIFTS to investigate the thermal stability of surface oxygen complexes [24]. Consequently, the following complexes were assigned to their corresponding temperature range of decomposition as listed in Table 2. The complexes are sorted in the order of increasing stability in the table, while their acidity follows the opposite trend. For instance, carboxylic acids are the least stable groups, yet they are the most acidic ones. Figure 10 illustrates the carbon-oxygen bonds that form these functionalities.

Abs. band, [cm^{-1}]	**Functional group**
1810	Esters (C=O)
1785	Carboxylic anhydrides (C=O)
1620	N=O vibration in CONO; chelated bond on two neighboring carbon sites
1600	N=O vibration in CONO; non-chelated bond on a single carbon site
1565	Asymmetric stretching vibration of NO_2 bound via its nitrogen atom
1485	Same as the band at 1340 cm^{-1} but for a more graphitic environment
1290-1350	Symmetric stretching vibration of NO_2 bound via its nitrogen atom
1220	C-O vibration in CONO

Table 1: Absorption bands and their corresponding functional groups for the reaction of Printex-U with NO_2 at 400 °C [23].

Two concurrent desorption peaks were observed at 160 °C for both NO and CO_2, therefore, those peaks are proposed to be due to the decomposition of an acidic functional group that fragments into NO and CO_2. However, in the IR spectrum of the sample reacted with NO_2 at 400 °C, no absorption band was observed at 1730 cm^{-1}, which is the characteristic of a C=O double bond. Consequently, the acidic functional group was considered

Functional group	Decomposition temperature, [°C]	Decomposition products
Carboxylic acid	100-400	CO_2 + OH
Lactone	190-650	CO_2
Carboxylic anhydride	350-627	CO_2 + CO
Phenol	600-700	CO + OH
Carbonyl	700-980	CO
Ether	700	CO
Quinone	700-980	CO

Table 2: Oxygenated functional groups on a carbonaceous surface and their thermal stability [24].

to be an intermediate that decomposes relatively fast. This intermediate is proposed to be formed in a two-step process: first NO_2 chemisorbs and leaves one oxygen atom on the carbonaceous surface at elevated temperatures. In this manner, a carbonyl group is formed (C=O), which is then oxidized by a neighboring chemisorbed NO_2 molecule. The essential conclusion drawn by Muckenhuber and Grothe was that two oxygen atoms from two different NO_2 molecules are incorporated in the acidic intermediate. It can, however, be debated whether the source of the second oxygen atom is restricted to be the neighboring chemisorbed oxygen. Alternative roots can be a second attack from an NO_2 molecule in the gas phase or a mobile oxygen atom chemisorbed on a different site [25, 26].

4.2 Promoting effect of water and oxygen

The presence of molecular oxygen considerably enhances the oxidation reaction of carbon with NO_2 [27, 28, 29]. Evidence suggests that molecular oxygen actively participates in oxygen transfer through irreversible chemisorption and the consequent formation of oxygenated surface complexes [29]. As illustrated in Figure 11, the promoting effect of water vapor (hereinafter denoted water) on NO_2-based oxidation is also significant particularly for CO_2 formation [1, 28, 29, 30].

In the presence of water, oxygen consumption from NO_2 has been observed to be greater than the total oxygen that exists in the reaction products, namely NO, CO, and CO_2 [29]. Therefore, the promoting effect of water has been proposed to be of a catalytic

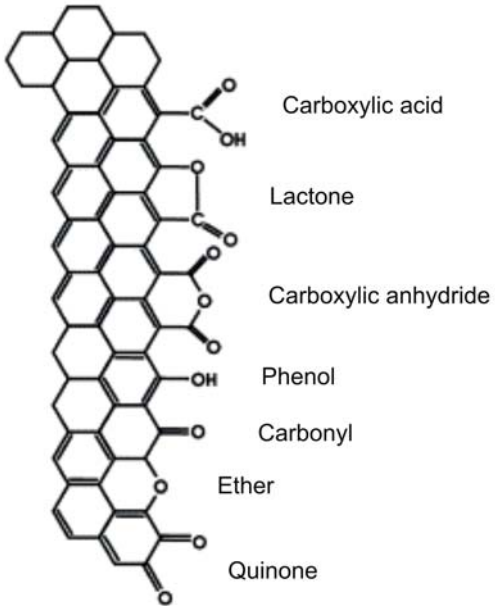

Figure 10: Oxygenated functional groups on a carbonaceous surface [24].

type, and the additional oxygen consumed from NO_2 has been attributed to the formation of HNO_2 and HNO_3 in the gas phase [29]. However, the formation of HNO_3 is an unlikely hypothesis due to the strong propensity of this compound to thermal decomposition at temperatures relevant to carbon oxidation [31].

Messerer et al. have reported that CO_2 formation is much more strongly enhanced in the presence of water, while CO formation is only slightly influenced [27]. They have proposed that either the water-gas shift reaction (WGS) in the gas phase influences selectivity or that water enhances the decomposition of surface oxygen complexes, such as carboxylic acids (which mainly decompose into CO_2 [24]). A study of water-assisted carbon oxidation with oxygen, has found a strong correlation between selectivity and the equilibrium constant of the WGS reaction [32]. However, both of the aforementioned studies consist of the catalytic oxidation of carbon, and at the temperature interval of diesel exhaust, the WGS reaction is unlikely to be influential in non-catalytic systems.

Above 3% water in the feed gas, changes in the inlet concentration of water have been reported to have no significant effects [27]. The effect of water has been observed to be dependent on temperature being less pronounced at higher temperatures [29]. Jacquot et al. have proposed a phenomenological model for the catalytic effect of water [29]. Their kinetic model consists of constant coefficients that express the effect of water in

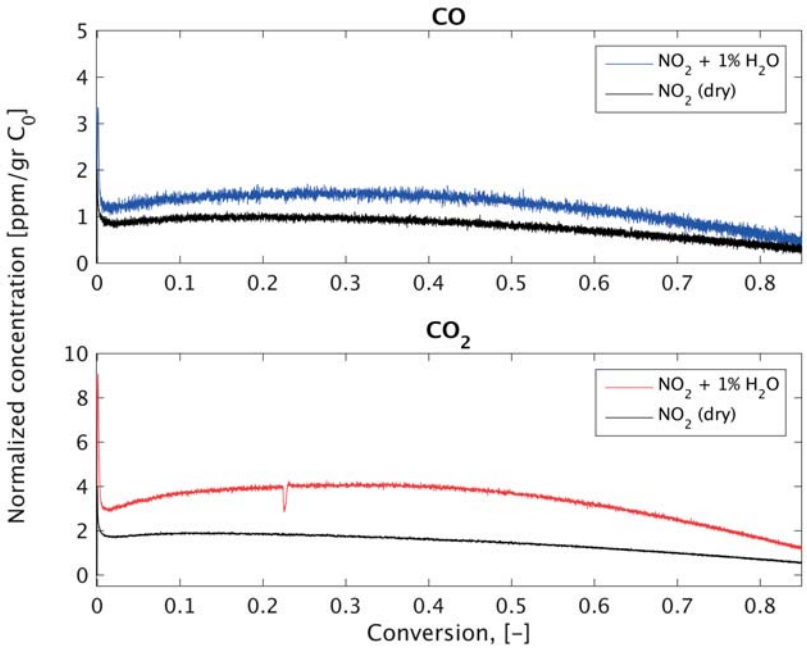

Figure 11: Promoting effect of water on NO_2-based oxidation (with 400 ppm NO_2, and 1% water at the inlet and at 400 °C).

an empirical way. This model was extended by Zouaoui et al. by using temperature-dependent coefficients instead [33]. However, the model is first-order with respect to carbon, and, therefore, it is incapable of predicting the acceleratory phase of the reaction; a phenomenon that gives rise to bell-shaped isothermal plots of the reaction rate. Section 4.4 will discuss an alternative approach to developing a kinetic model that can handle such cases.

Figure 12 shows a synergistic effect that was observed when both oxygen and water were simultaneously present in the gas phase along with NO_2. Considering the abundance of water and oxygen in diesel exhaust, it is of great importance to take their promoting effect into consideration in studies of automotive soot oxidation. In the research conducted within this thesis, the promoting effect of water and oxygen were investigated experimentally, and a global kinetic model was developed that can be successfully fitted to the observed rate of reaction. Furthermore, experimental evidence was found that highlights the role of surface oxygen complexes in explaining the observed promoting effect of water. An evaluation of [-O-] and [-N-] balance was used to examine the characteristics of the promoting effect of water and oxygen.

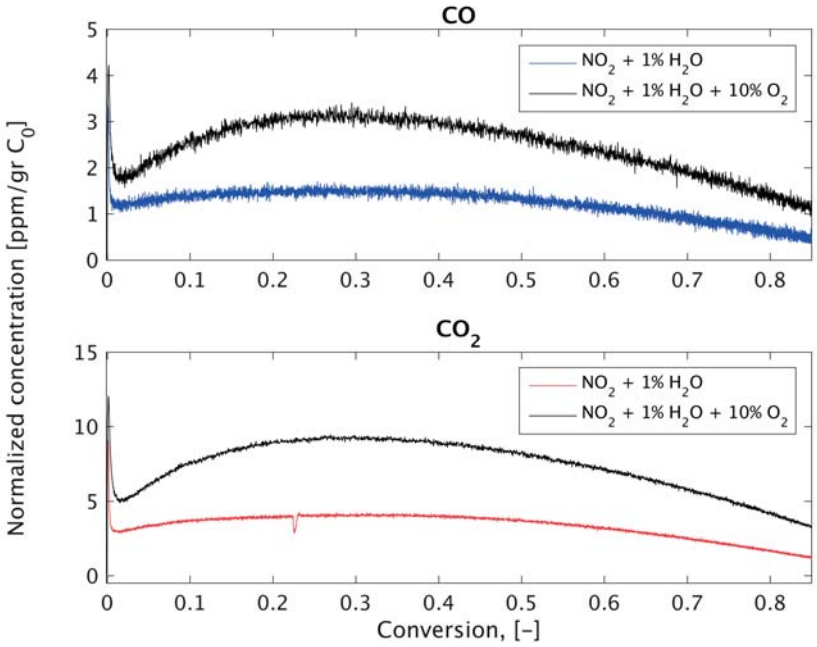

Figure 12: Synergistic effect of oxygen, water, and NO_2 on carbon oxidation (with 400 ppm NO_2, 10% O_2, and 1% water at the inlet and at 400 °C).

4.3 Kinetics of carbon oxidation

A crucial step in carbon oxidation is the chemisorption of oxygen on carbon, therefore, oxygen access strongly controls the observed rate of oxidation. As discussed in Section 1.1, the porous structure of carbon undergoes significant changes with progressive conversion, which, in turn, cause oxygen access to be a strong function of conversion. In this manner, the kinetic parameters of the oxidation reaction have been observed to be conversion-dependent [34]. In particular, the relationship between changes in surface area and variations of mass (or equivalently volume) with conversion determines the reaction order of carbon, which varies between two extremes of 2/3 and 1 (neglecting the initially negative reaction order of carbon. See Section 5.5.1).

For highly porous material, the surface area shrinks linearly with mass resulting in a reaction order of unity. On the other hand, the surface area of a compact particle, which shrinks from its external surface only, decreases slower than mass, which gives rise to a

reaction order of 2/3 for mono-dispersed spherical particles[1].

It has been suggested that a first-order model can adequately represent the observed oxidation rate of diesel soot samples [35], which relaxes the conversion dependence of reactivity and, thus, simplifies the models for filter regeneration. However, it is commonly observed that neither a 2/3 nor a first-order model can properly explain the observed rate of oxidation over the entire conversion interval [36, 37]. Experimental evidence shows that the reaction order of carbon is not constant and varies significantly with carbon conversion [38]. In fact, reaction rate profiles are typically bell-shaped and exhibit a maximum at low to medium degrees of conversion.

4.3.1 Available surface area and reactivity

The kinetics of carbon oxidation can be formulated according to the following rate expression:

$$r = NS_a k(T)h(p_i) \tag{3}$$

where r is the rate of carbon combustion in $(\frac{mol}{grC.s})$, N is the surface concentration of active sites $(\frac{mol}{m^2})$, S_a is the specific surface area $(\frac{m^2}{grC})$, which is a function of conversion, $k(T)$ represents the intrinsic rate constant of the reaction, which is a function of temperature, and h is a function that accounts for the concentration dependency of the rate [39].

Specific surface area may change appreciably during the course of combustion due to pore growth, collapse, and coalescence (see Section 1.1). Specific surface area is generally either a monotonically decreasing function of burn-off or it exhibits a maximum. Both theoretical and empirical attempts have been made to model changes in specific surface area with conversion. Examples include the random pore model of Bhatia and Perlmutter, power law models, and percolation models [40, 41, 42, 43].

The total surface area (TSA) of carbonaceous matter can be classified as either the basal plane (BP), or the active surface area (ASA). The former is inactive towards chemisorption of gas-phase species, while the latter consists of the edge planes and the defect sites where activated chemisorption predominantly occurs.

[1]For poly-dispersed particles, any reaction order of larger than 2/3 can be obtained due to the much higher reaction rate of the smaller particles.

The active site density in Eq. 3 is strongly dependent on the type of carbon and can vary also during the reaction. More importantly, it has been argued that the ASA is very likely to be dependent on temperature as well considering the fact that at higher temperatures more sites can participate in activated chemisorption [44]. Additionally, as discussed in Section 4.1, activated chemisorption results in the formation of oxygenated complexes of which a certain fraction remains stable at the reaction's temperature. Therefore, it can be argued whether the ASA would be the most relevant quantity for normalizing the observed rate of oxidation. Although it has been successfully used to obtain an intrinsic rate constant for graphitized carbons, ASA has failed to correlate the reactivity of less-ordered carbonaceous matter [45, 46, 47, 48].

The fraction of the ASA on which the oxygenated complexes, at the reaction temperature, undergo decomposition to form the reaction products, i.e. CO and CO_2, is called the reactive surface area (RSA). The remaining of the surface complexes are only temporarily stable at the same temperature until the surrounding carbon atoms leave the carbon lattice because of the ongoing reaction. In fact, changes in the surrounding environment cause surface oxygen complexes to restructure as can be understood from Figure 10. The sites that are covered with surface complexes form the unreactive surface area, (URSA).

It is fundamentally more relevant to correlate carbon's reactivity using the RSA. To this end, transient kinetic methods are the only means that can reveal the true reactive site density [39]. By integrating the area under the transient decay of the gasification product, i.e. CO, of three char samples, Jiang and Radovic have calculated their RSA [45]. The thus-obtained rate constants were observed to be invariant with respect to conversion. Using the same methodology, Nozaki et al. also correlated the reactivity and the number of reactive sites of five char samples [49]. They have also pointed out the presence of two different time constants in the transient decay profile.

Due to their particular relevance to studies of carbon oxidation, an overview of transient kinetic methods is briefly outlined in the next section.

4.3.2 Transient kinetic methods

In transient methods, a system at rest is stimulated using a known perturbation followed by monitoring the response of the system while it approaches equilibrium [50]. The

chief advantage of these methods lies in the fact that at steady state, all mechanistic steps proceed at the same rate, and, therefore, it is not possible to distinguish the rate-determining step(s). Consequently, different mechanisms can fit the experimental results obtained solely under stationary conditions. Therefore, transient methods must be used to propose and verify the realistic mechanisms for surface reactions and to reject the unlikely ones [51].

In the research conducted herein, step-response (SR) experiments, more specifically, the transient decay of CO and CO_2 during the relaxation period of each step, were used to investigate the mechanistic aspects of carbon oxidation. One of the most restricting factors in transient experiments is the response time of the detector, which directly determines how fast processes can be monitored with the available instrument [52]. In Paper II, the gas cell of an FTIR analyzer was characterized, which revealed that the most drastic loss of temporal resolution was due to the hydrodynamic dispersion inside the gas cell. In the characterized setup, approx. 94% of the variance of a residence time distribution originated from the dispersion in the gas cell [11]. Using a deconvolution algorithm to circumvent this limit is, therefore, of considerable importance in transient analyses.

The interested reader is referred to the literature for a detailed elucidation of transient methods in general [50, 51, 53, 54, 55, 56, 57, 58, 59, 60]. The study by Kobayashi and Kobayashi makes use of a qualitative interpretation of various transient response modes [55, 56]. Transient studies of carbon gasification are also of particular relevance [44, 45, 49, 61, 62, 63, 64, 65, 66].

4.4 A global kinetic model

The approach that was chosen in Papers I and V to develop a global kinetic model for carbon oxidation was to express the observed reaction rate as a function of Arrhenius parameters along with an extra term, a so-called reaction model, that accounts for conversion-dependencies (see Section 5.5.5) [34].

In Paper I, a multi-step kinetic model was proposed that consisted of a third-order Avrami-Erofeev model to account for the conversion dependencies. The proposed model could fit the experimental results of both the isothermal and temperature-programmed

oxidation of Printex-U with oxygen and NO_2 [34].

An Avrami-Erofeev type model is a theoretical framework that explains the kinetics of phase change using both a nucleation and a growth process [67, 68]. In contrast to processes like crystallization, the formation of a new phase is typically not involved in solid-state decomposition (as in e.g. carbon oxidation). Nevertheless, an Avrami-Erofeev model has been regarded as a generalized framework for modeling both nucleation-driven systems and the more complex ones involving diffusion and interface reaction [69].

As found in HRTEM images of various carbonaceous samples, oxidation creates new edge sites on the graphitic lamellae of carbon. Subsequently, these new sites escalate providing oxygen access to the graphitic sub-layers as well [70]. Moreover, experimental studies show that the presence of water causes the surface area of diesel soot to increase faster particularly above 20% conversion [71].

Müller et al. have considered a number of processes including initial surface oxidation, the formation of small pores followed by pore enlargement, and eventually shrinkage of particles to explain the complexity of the overall oxidation reaction [72].

Nucleation-growth models have been extended by Bhatia and Perlmutter who have developed a random pore model (RPM) that accounts for changes in the porous structure of carbon with progressive conversion [40]. The RPM is a mathematical model that assumes cylindrical pores with random size distribution. Such pores grow and collapse with progressive conversion. The model can predict both sigmoid and monotonic reaction rate profiles using a structure parameter. In Paper V, a kinetic model was developed for NO_2-based oxidation in the presence of both water and oxygen using the RPM to account for the development of the porous structure of carbon with progressive burn-off. The reaction rate equations r_1 and r_2 were formulated as:

$$r_1 = k_1 \left([NO_2] \times 100\right)^{\beta_1} f(X) \tag{4}$$

$$r_2 = k_2 \left([NO_2] \times 100\right)^{\beta_2} f(X) \tag{5}$$

$$f(X) = (1 - X)\sqrt{1 - \psi \ln (1 - X)} \tag{6}$$

where r_1 and r_2 ($\frac{mol}{grC.s}$) are the rate of formation of CO and CO_2, respectively. In

the above equations, $f(X)$ is the reaction model according to the RPM, which can be considered to be equivalent to $N.S_a$ in Eq. 3, square brackets denote gas-phase concentration ($\frac{mol}{m^3}$), β_j are the reaction orders of NO_2, and k_j are rate constants according to the Arrhenius expression. To reduce the correlation among the parameters, the concentration of NO_2 was scaled by a factor 100 in Eqs. 4 and 5. In particular, to reduce the correlation between the pre-exponential factors and activation energies, rate constants were centered on a reference temperature of $T_{ref.} = 400$ °C:

$$k_j = A_j \exp\left[-\frac{E_{a,j}}{R}\left(\frac{1}{T} - \frac{1}{T_{ref.}}\right)\right] \tag{7}$$

4.5 Reactor model

A reactor channel was discretized into a number of tanks-in-series in order to resolve the concentration gradients of NO_2 along the channel. About 50-55 tanks were estimated to account for Taylor dispersion [73], however, using more than 30 tanks was practically unnecessary as no significant changes were observed.

By using the guidelines suggested by the characterization study of the experimental setup, temperature gradients within the reactor could be minimized to less than 5 °C. It was experimentally observed that temperature increase due to the reaction was negligible (less than 3 °C). Consequently, the reactor operation was assumed to be isothermal, and the energy equation was not included in the reactor model. Therefore, the following material balance equations were formulated and solved for each tank:

$$V_t \frac{d[CO]_i}{dt} = F\left([CO]_{i-1} - [CO]_i\right) + r_1 m_{C,i} \tag{8}$$

$$V_t \frac{d[CO_2]_i}{dt} = F\left([CO_2]_{i-1} - [CO_2]_i\right) + r_2 m_{C,i} \tag{9}$$

$$\frac{dm_{C,i}}{dt} = -(r_1 + r_2) m_{C,i} MW_C \tag{10}$$

$$V_t \frac{d[NO_2]_i}{dt} = F\left([NO_2]_{i-1} - [NO_2]_i\right) - (r_1 + 2r_2) m_{C,i} \tag{11}$$

where $m_{C,i}$ (gr) is the remaining mass of carbon in tank i, V_t (m^3) is the volume of each tank, MW stands for molecular weight, F $(\frac{m^3}{s})$ is the volumetric flow rate at the pertaining temperature, and square brackets denote the gas-phase concentration of species $(\frac{mol}{m^3})$.

4.6 Population balance modeling for tracking conversion

A reaction order in carbon of other than unity implies that the conversion history of soot plays a major role in predicting filter loading during regeneration cycles. A population-balance model (PBM) was formulated that keeps track of the conversion history of carbon while the computational cost is easily affordable on an ordinary desktop computer (the computational time is within seconds).

The PBM assumes that the temporal change in soot mass loading inside a filter channel is balanced by the freshly-loaded soot and a continuous oxidation reaction that occurs inside the channel, according to Eq. 12 [34].

$$\frac{dm}{dt} = \eta\dot{m} - r \tag{12}$$

Here, m is the soot mass loading, r is the conversion-dependent, reaction rate equation, $\dot{m}$ is the mass flow rate of soot entering the filter, and η is the filter efficiency that can be assumed to be approx. 1.

To solve the population balance equation, the following algorithm is proposed assuming that the fresh soot enters the filter in batches of equal mass. This assumption is merely for the sake of simplicity, and the algorithm can easily be extended to a more general case with random mass distribution for the soot inflow.
Starting with a clean filter at t_0, at each time-step, a batch of soot with a mass of m_0 enters the filter. The batches that were added in previous time-steps undergo shrinkage due to oxidation, the magnitude of which is determined by integrating the reaction rate equation. Therefore, the following lower-triangular matrix that holds the remaining mass of each batch at each and every time-steps can be constructed. Consequently, the soot mass loading at each time-step is the sum of all elements on the corresponding row of the matrix:

$$
\begin{array}{c|ccccc}
t_0 & m_0 & 0 & 0 & \cdots & 0 \\
t_1 & m_0 & m_1 & 0 & \cdots & 0 \\
t_2 & m_0 & m_1 & m_2 & \cdots & 0 \\
\vdots & \vdots & \vdots & \vdots & \ddots & \vdots \\
t_n & m_0 & m_1 & m_2 & \cdots & m_n
\end{array}
$$

For a more general case with a randomly distributed mass of inflow particles, a lookup table can be constructed ahead of time by integrating the reaction rate equation from t_0 to some t at which the death condition for a population, i.e. the complete burn-off for a batch of soot, is fulfilled. Therefore, at each time-step, the lookup table can be used to calculate the remaining mass of each batch that entered the filter in previous time-steps. This algorithm can easily be implemented in more sophisticated flow models, e.g. a computational fluid dynamics simulation of a filter channel. However, it should be noted that the above-mentioned analysis is restricted by an underlying assumption of constant temperature and constant concentration of NO_2. Under concentration and temperature gradients that are typically present in a filter, a much more complex algorithm must be developed that can account for the effect of transient concentration and temperature distributions on the rate of oxidation.

4.7 Performance gain for computational kinetic modeling

Developing computational kinetic models often involves two subroutines: i) a parameter estimation algorithm; and ii) an ODE solver. Together with a main function as an entry point that initializes the computations, these three subroutines interact as depicted in Figure 13. The hierarchy of the caller functions starts with the main function. As examples for MATLAB-based models, the specific functions that invoke another subroutine are shown in italic type. Therefore, it is clear that the subroutine that evaluates the system of ODEs is the one that is called the most thereby forming a potential bottleneck of the computations.

To gain performance, MATLAB, which is an interpreted environment, was interfaced with C using a MEX file that includes the implementation of the system of ODEs. After being compiled, a MEX file is dynamically loaded, which substantially reduces the computational time (more than 80% in this study). For more information about setting up

Figure 13: A flow-chart describing the sequence of function invocations in the computational model.

MEX files see reference [74].

Multi-threading can also help reduce the computational time by, for instance, distributing the evaluation of the sum of squared errors for different experimental conditions among a pool of threads executing in parallel [75]. In MATLAB, this was implemented using the `spmd` function. In the present case, however, a multi-threaded implementation could not surpass the performance of a serial code (both of which invoke MEX functions). The reason was found to be due to the substantial overhead associated with the iterative creation of the pool of workers, i.e. the initialization of the `spmd` function itself.

5

Results and Discussion

This section summarizes the findings of this study including the main outcomes of Papers I-V.

5.1 Temperature profiles inside the reactor

Based on the characterization of the experimental setup, a number of guidelines were proposed to improve the quality of measurements [11]:

1. Radiation shielding to prevent heat loss to the cool walls of the outlet region by inserting an inert monolith downstream of the reactor
2. Adjusting the heating coil to create a high- and a low-heat flux region. The idea is to allow the added heat in the high-heat flux region to be evenly distributed in the radial direction. Therefore, the heat in the low-heat flux region is mainly supplied to the extent that compensates for loss
3. Inserting an inert monolith upstream of the reactor in order to obtain a better radial temperature profile. This inert monolith would simultaneously protect the thermocouples from the thermal irradiation from the quartz wall and the heating coil
4. Proper insulation, especially of the outlet part of the setup

These guidelines are illustrated in Figure 14 with the photographs taken during the startup of an experiment.

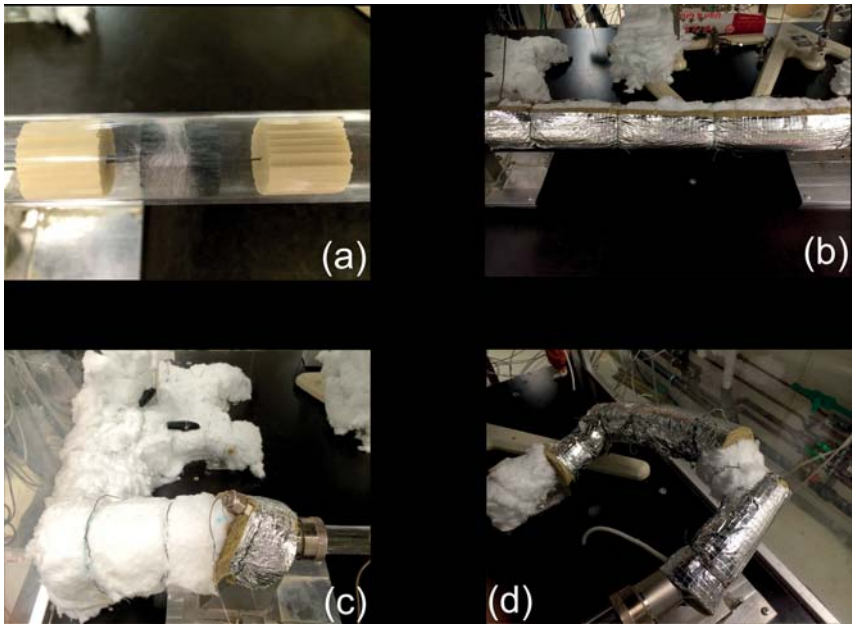

Figure 14: Implementation of the proposed guidelines for improving the quality of experimental data. a) Placement of inert monoliths, b) proper insulation of the reactor tube, c) insulation of the outlet part, d) insulation of the pre-heating line.

Figure 15 depicts the results of CFD simulations of the reactor setup with and without the inert monoliths [11]. The inert monolith in the upstream has a higher thermal conductivity than that of the gas phase, and it also provides a larger surface area for heat transfer. Therefore, it is mainly effective to dissipate radial temperature gradients. In contrast, the inert monolith downstream acts as a radiation shield for the reactor and helps reduce axial temperature gradients to a great extent. A comparison of the middle and the bottom panels in Figure 15 shows how these axial gradients are shifted further downstream by incorporating the inert monolith in the rear.

5.2 Residence time distribution

Empty-reactor experiments show that a significantly distorted response can be detected with an FTIR analyzer. Figure 16 depicts the observed signal distortion in one such experiment with a step-change to 500 ppm NO_2 as the tracer at the inlet of the quartz tube. This can substantially restrict transient measurements, which require a very high temporal resolution.

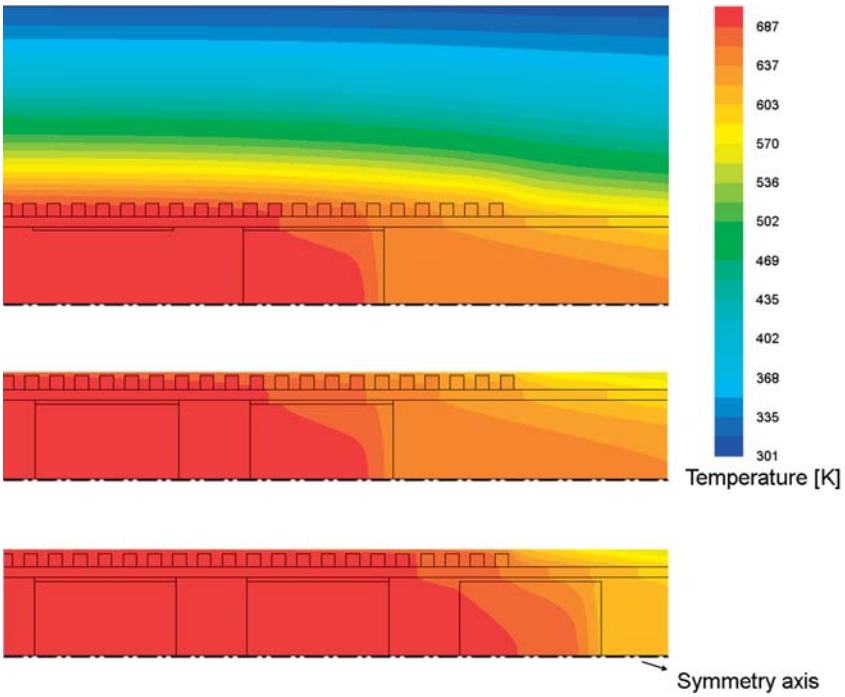

Figure 15: The role of the inert monoliths in the up- and downstream of the reactor. a) A single reactor, b) an inert monolith in the upstream, c) inert monoliths confining the reactor [11].

Therefore, analyzing residence time distribution in the reactor system was a central part of the characterization study of Paper II. The observed signal distortion originates from the hydrodynamic dispersion of a concentration front throughout the setup. Considering the reactor setup as a linear, time-invariant system, the time-dependent outlet concentration obeys the following convolution integral:

$$\int_0^t x(t)g(t-t')dt' = y(t) \tag{13}$$

where x and y denote the input and the detected signals, respectively. The function $g(t)$ represents the residence time distribution in the setup, which can be calculated by differentiating the normalized response of the system to a step input with respect to time [76]. A schematic illustration of the concept is given as the block diagram in Figure 17.

Using the Aris-Taylor equation for hydrodynamic dispersion in the tubular parts of the setup, i.e. the quartz tube and the piping, it was found that about 6% of the overall broadening stems from the quartz tube, and the contribution of the piping is negligible

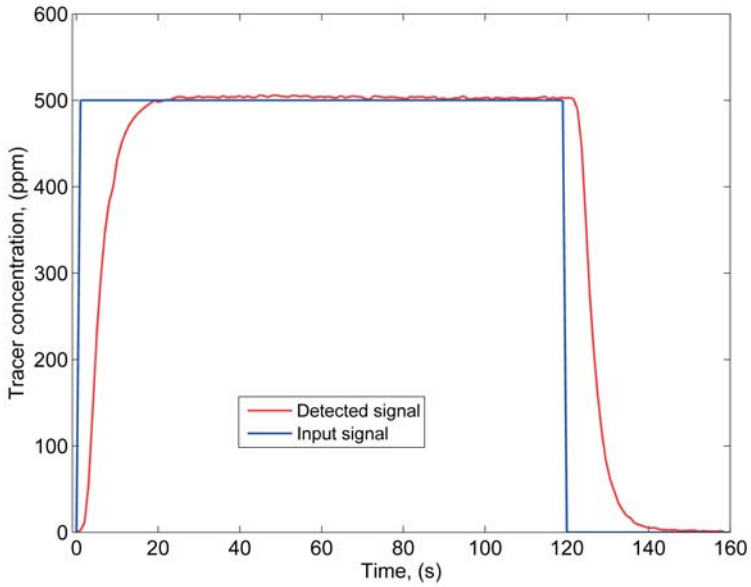

Figure 16: The observed distortion of a step signal in an empty-reactor experiment [11, 15].

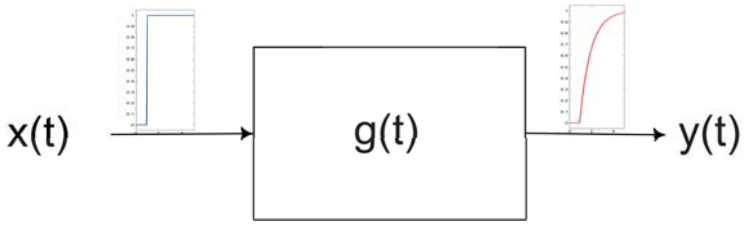

Figure 17: A block diagram of the reactor setup along with the input and the distorted output signals.

[11, 77, 78]. Therefore, the remaining approx. 94% of the variance of the system's RTD is due to the gas cell of the FTIR analyzer. In other words, the function $g(t)$ in Eq. 13 lumps together the intrinsic RTD of the quartz tube and that of the gas cell of the FTIR analyzer. In experiments with an ongoing chemical reaction, a monolithic reactor is normally placed quite close to the outlet of the quartz tube. Consequently, the gas cell becomes the only significant part that causes the distortion of the detected concentration of the reaction products.

Two approaches are proposed to acquire the intrinsic RTD of the gas cell. One is a transient CFD simulation of the gas cell, which has been elaborated in Papers II and IV.

This approach directly yields the RTD of the cell [11, 22]. Alternatively, for any reactor setup, deconvolution can be used to reconstruct the RTD of the region of interest from the results of pulse- or step-response experiments. To this end, the following are required: i) the detected concentration of a tracer at the outlet, i.e. $y(t)$; ii) the residence time distribution of all the parts that are located before the region of interest, i.e. the quartz tube in this specific problem. In this manner, deconvoluting the two functions will give the transfer function of the region of interest.

The RTD of the quartz tube can be estimated as a Gaussian function according to the Aris-Taylor analysis of axial dispersion in a tube. The calculated variance for the tube was about 0.66 s^2, which is fairly comparable to the result obtained from a CFD simulation that predicted a variance of about 0.62 s^2 [11]. Figure 18 depicts the corresponding Gaussian distribution that represents the RTD of the quartz tube.

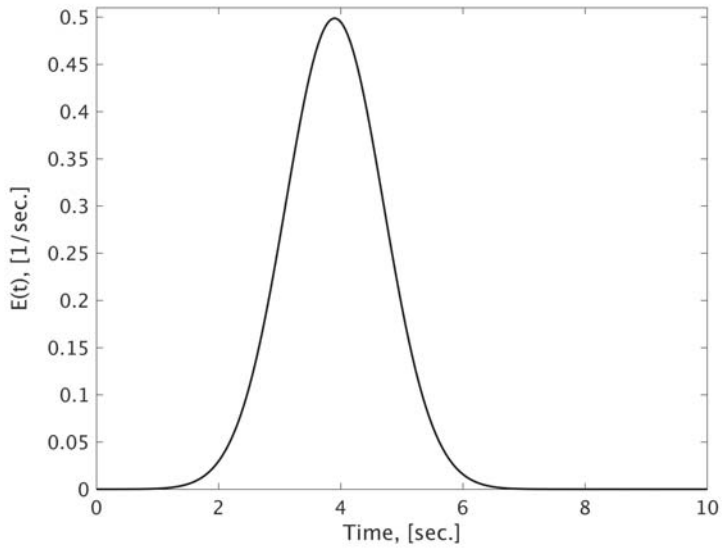

Figure 18: The normalized residence time distribution of the quartz tube.

The advantage of the former approach is that solving an ill-posed inverse problem of deconvolution and its consequent burden is avoided, but that typically comes at the price of greater computational effort. Figure 19 shows the reconstructed RTD of the gas cell using both methods. For the sake of comparison, the RTD of a well-mixed vessel with a response time of 3.08 s has been included in Figure 19. The CFD simulation was terminated slightly earlier than 30 s to make its computational time affordable.

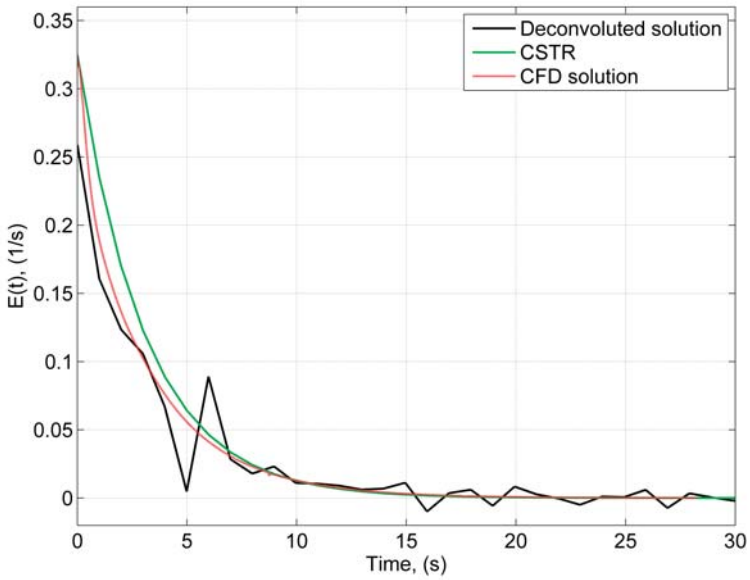

Figure 19: The normalized residence time distribution of the gas cell obtained using the deconvolution algorithm (black) and a CFD simulation (red). The green curve compares the results with the RTD of a CSTR with a response time of 3.08 s.

5.3 A systematic error in transient experiments

The notion of residence time distribution implies that a certain time interval needs to be lapsed before a homogeneous concentration profile has pertained throughout an entire vessel. In FTIR-based measurements, this would mean that the transient part of a concentration profile would coincide with the time interval it takes for a homogeneous concentration profile to fill in the gas cell. Therefore, the measurements are prone to a systematic error during this time interval if the gas-phase components have non-linear IR absorption behavior. This is due to the fact that an integrated absorbance of the IR beam is used in the detector to predict the prevailing concentration inside the gas cell. One such compound with non-linear IR absorption that is of importance for studies of carbon oxidation is carbon monoxide. Nitric oxide exhibits a similar behavior too, but at much higher concentration levels than what exists in diesel exhaust. Using CFD simulations, the study conducted in Paper IV demonstrates this systematic drift for both gases.

It is noteworthy that the magnitude of the error is dependent on the inlet concentration of the cell as well as the molecular diffusivity of the species. The latter is only significant for laminar flows. As a remedy, a compartment model calibrated to the results of the CFD simulations was proposed to be developed. A compartment model can be much more easily implemented in a non-linear regression analysis. The model was subsequently developed within a master thesis project co-supervised by the author [79].

5.4 Transient kinetic study and the mechanism of carbon oxidation

A transient experiment was conducted at 350 °C by pulsing 500 ppm NO_2 at the inlet of the reactor system. The pulse duration time was chosen to be 2 minutes to avoid the significant changes in each step caused by carbon conversion. Each step was followed by a relaxation period of 3 minutes during which the transient decay of CO, CO_2, NO, and NO_2 were monitored. The recorded response of those species during an arbitrarily chosen step was singled out and plotted in Figure 20.

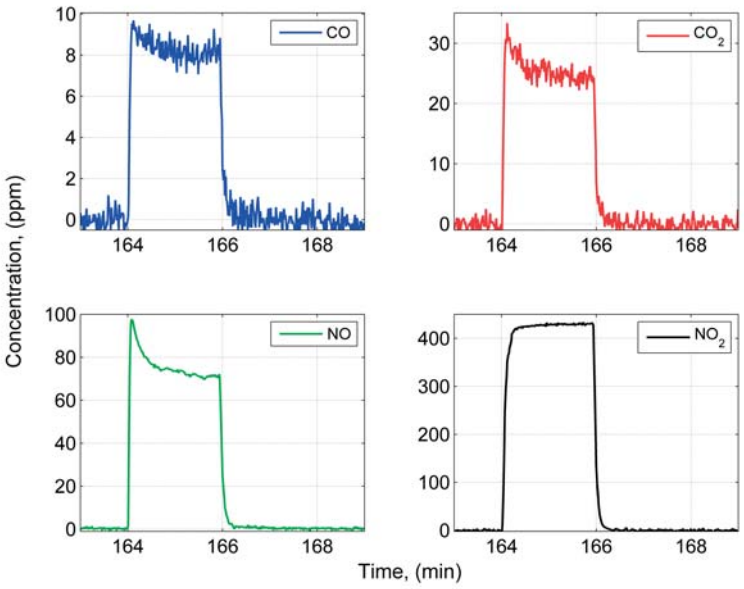

Figure 20: Transient concentration profiles of the products of a carbon-NO_2 reaction during a typical step-response experiment.

When the reactive gas is switched to inert, the graphs in Figure 20 show that there are at least two distinct, parallel processes with markedly different response times that are responsible for CO and CO_2 evolution. There is a fast process that is responsible for almost 80% of the observed rate of formation of products, and a slow process that shows a tailing profile over the relaxation period. A mechanism has been proposed to explain these two processes using a different type of oxygen adsorbed on the basal plane of carbon as epoxide [26, 80].

Due to its much higher reactivity and possibly also due to the origin of this type of oxygen, the concentration of epoxide oxygen on the basal plane is comparably lower than the more stable oxygenated complexes (cf. Table 2 in [44]). Therefore, it can be assumed that this type of complex is formed, in a reversible step, by means of oxygen hopping between the edge and basal planes. Consequently, the postulated mechanism, with minor adjustments for the interaction between NO_2 and carbon, reads:

$$C_f + NO_2 \rightarrow NO_{(g)} + C(O) \tag{14}$$
$$2C(O) \rightleftarrows C_b(O)C(O) + C_f \tag{15}$$
$$C_b(O)C(O) \rightarrow CO_{(g)} + C(O) \tag{16}$$
$$C(O) \rightarrow CO_{(g)} + C_f \tag{17}$$
$$C_b(O)C(O) \rightarrow CO_2 + C_f \tag{18}$$
$$2C(O) \rightarrow CO_2 + C_f \tag{19}$$

In this reaction network, a C(O) complex represents the oxygen-containing complexes on the edge plane (cf. Tables 1 and 2 and Figure 10), while C_b(O)C(O) denotes the off-plane bond between oxygen and carbon in the form of an epoxide, and C_f represents a vacant site.

When the reactive gas is switched to inert, Eq. 14 no longer contributes to the formation of complexes. Instead, the already formed oxygenated complexes are consumed according to Eqs. 15 through 19. Therefore, the observed rate of formation of CO and CO_2 during the relaxation period can be explained as follows:

$$r_{CO} = k_{16}[C_b(O)C(O)] + k_{17}[C(O)] \tag{20}$$

$$r_{CO_2} = k_{18}[C_b(O)C(O)] + \frac{1}{2}k_{19}[C(O)]^2 \tag{21}$$

The following ordinary differential equations (ODEs) describe the temporal changes in the concentration of vacant and oxygenated carbon sites with k' denoting the rate constant of a backward reaction:

$$\begin{aligned}\frac{d[C(O)]}{dt} =& -2(k_{15}+k_{19})[C(O)]^2 + 2k'_{15}[C_b(O)C(O)][C_f] + \\ & k_{16}[C_b(O)C(O)] - k_{17}[C(O)]\end{aligned} \tag{22}$$

$$\frac{d[C_b(O)C(O)]}{dt} = \frac{1}{2}k_{15}[C(O)]^2 - k'_{15}[C_b(O)C(O)][C_f] - (k_{16}+k_{18})[C_b(O)C(O)] \tag{23}$$

$$\frac{d[C_f]}{dt} = \frac{1}{2}(k_{15}+k_{19})[C(O)]^2 + k_{17}[C(O)] + k_{18}[C_b(O)C(O)] - k'_{15}[C_b(O)C(O)] \tag{24}$$

As a preliminary analysis, the mechanism was fitted to the experimentally-measured rate of the formation of the products during the relaxation period of a transient experiment, as shown in Figure 21. The governing equations were implemented in the MATLAB environment, and its built-in function `lsqnonlin` was used for parameter estimation. The system of ODEs was numerically integrated using MATLAB's stiff solver `ode15s`. The parameters were, in general, weakly correlated.

The possibility for oxygen to be bonded to the basal plane is subject to criticism. Nevertheless, sufficient for our analysis is that the decaying profile of the oxidation products, i.e. CO and CO_2, cannot be fitted with a simple, first-order process. This will be discussed further in Section 5.5.5 in connection with the kinetic study of carbon oxidation.

5.5 Kinetic study under realistic exhaust conditions

The following sections include a kinetic study of carbon oxidation with NO_2 in the presence of water and oxygen. The role of surface oxygen complexes with respect to the observed promoting effect of water will be discussed, and the global kinetic model will be

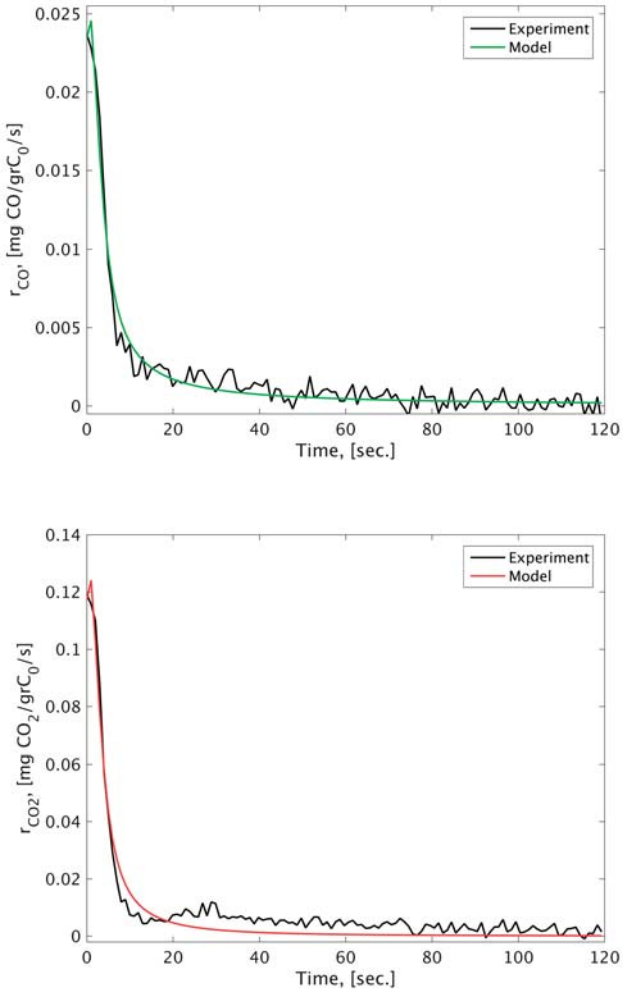

Figure 21: Experimentally measured versus the fitted model (Eqs. 15 through 19) for the decaying profile of the oxidation products CO (top) and CO_2 (bottom).

examined. To keep track of the age distribution of the carbonaceous phase, a population balance model will be formulated, and last, an application of the kinetic model for design optimization will be illustrated.

The design of experiments and the relating information that will be referred to in the coming sections are summarized in Table 3.

No.	$[NO_2]_{in}$ (ppm)	T [°C]	$[H_2O]$ (%)	$[O_2]$ (%)	$[\text{-O-}]_{in}$ $(\frac{mmol}{grC_0.s})$ ± 0.02	$[\text{-O-}]_{out}$ $(\frac{mmol}{grC_0.s})$ ± 0.02	$[\text{-N-}]_{in}$ $(\frac{mmol}{grC_0.s})$ ± 0.01	$[\text{-N-}]_{out}$ $(\frac{mmol}{grC_0.s})$ ± 0.01	$[CO]/[CO_2]$ $(-)$	$[\text{-O-}]/[\text{-N-}]$ $(-)$
1	500	450	5	3	0.29	0.25	0.15	0.12	0.40	2.0
2	300	450	5	3	0.17	0.14	0.09	0.07	0.41	2.1
3	500	350	5	3	0.33	0.32	0.17	0.16	0.26	2.0
4	300	350	5	3	0.17	0.16	0.08	0.08	0.26	2.0
5*	400	400	5	3	0.27	0.24	0.13	0.12	0.32	2.0
6	300	350	5	0	0.10	0.10	0.05	0.05	0.31	2.0
7*	300	450	5	0	0.14	0.13	0.07	0.07	0.39	2.0
8	500	350	5	0	0.25	0.24	0.12	0.12	0.32	2.0
9*	500	450	5	0	0.21	0.20	0.11	0.10	0.42	1.9
10	400	400	5	0	0.16	0.15	0.08	0.08	0.33	2.0
11	500	450	0	0	0.35	0.32	0.18	0.16	0.53	2.0
12	300	450	0	0	0.21	0.19	0.11	0.10	0.51	2.0
13*	500	350	0	0	0.30	0.29	0.15	0.15	0.32	2.0
14	400	400	0	0	0.25	0.24	0.13	0.12	0.39	2.0

Table 3: Design of experiments. The net inflow and outflow of oxygen and nitrogen included in columns 6-9 were calculated using averaged values around 50% burn-off (see Section 5.5.2 for more information). * *Replicated experiments.*

5.5.1 Reaction order of carbon

Although the concentration of NO_2 is subject to variations with both conversion and axial position along a reactor channel, a preliminary analysis of the reaction order of carbon can be conducted by examining the logarithm of reaction rates versus the logarithm of remaining carbon. Figures 22 through 24 show the results of such analyses under different oxidizing environments. The reaction rates in these graphs were normalized by the initial

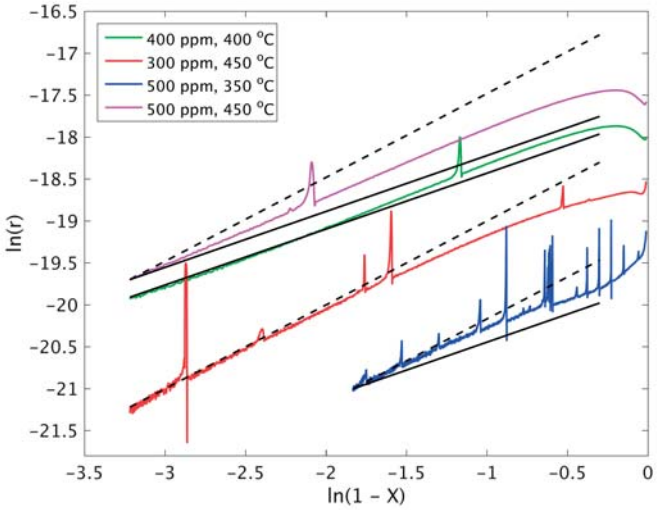

Figure 22: Plots of the reaction order in carbon for the C + NO_2 reaction. Dashed lines show first-order decay, and the black, solid line corresponds to a shrinking core model.

mass of carbon. The noise in the data was smoothed using a Savitzky-Golay filter to enhance visual interpretation [81]. It was observed that the reaction order of carbon was initially negative, which progressively increased with conversion.

As shown in Figure 23 for the C + NO_2 + H_2O reaction, the reaction order of carbon increased to around 2/3 at 45-80% burn-off and reached unity at the final stages of the reaction, i.e. above 85% conversion. On the other hand, no particular trend could be generalized for the C + NO_2 reaction, as reaction orders of both 2/3 and unity were observed at various stages of conversion (Figure 22). Figure 24 shows that in the presence of both H_2O and O_2 along with NO_2, the reaction order in carbon is close to 2/3 over 65-90% conversion depending on temperature and inlet concentration of NO_2.

5.5.2 Oxygen and nitrogen balance

The rates of inflow and outflow of [-O-] and [-N-] are listed in columns 6 through 9 of Table 3 using averaged values around 50% conversion. A window of 40 data points was chosen for averaging. The tolerances were calculated using standard deviations of the repeated experiments. In experiments 1 through 5, molecular oxygen was excluded from the calculations as there was no measured concentration available. Therefore, the rates of inflow and outflow of species were calculated according to Eqs. 25 through 28 by

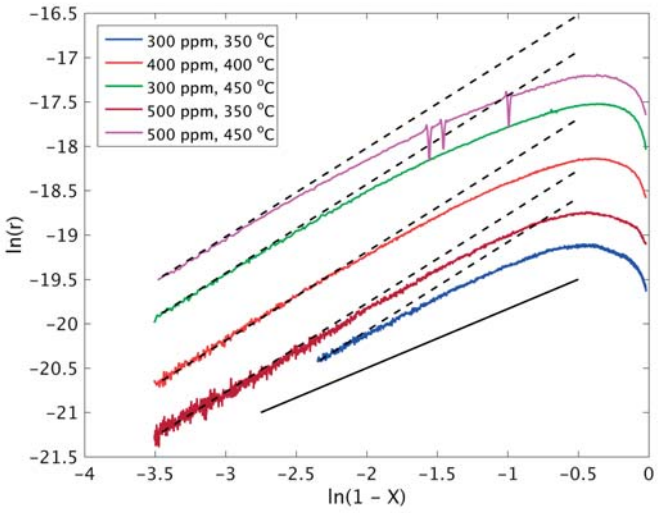

Figure 23: Plots of the reaction order in carbon for the C + NO_2 reaction in the presence of water. Dashed lines show first-order decay, and the black, solid line corresponds to a shrinking core model.

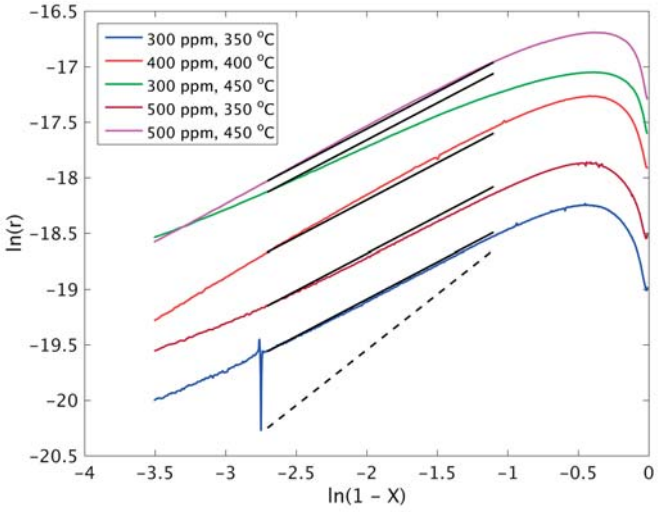

Figure 24: Plots of the reaction order in carbon for the C + NO_2 reaction in the presence of both water and oxygen. Dashed lines show first-order decay, and the black, solid lines correspond to a shrinking core model.

considering that NO_2 decomposition to $NO + \frac{1}{2}O_2$ has a negligible effect in the absence of a catalyst:

$$[-N-]_{in} = \langle [NO_2]_{in} \rangle \frac{FP}{RTm_{C,0}} \tag{25}$$

$$[-N-]_{out} = (\langle [NO_2]_{out} \rangle + \langle [NO]_{out} \rangle) \frac{FP}{RTm_{C,0}} \tag{26}$$

$$[-O-]_{in} = 2 \times \langle [NO_2]_{in} \rangle \frac{FP}{RTm_{C,0}} \tag{27}$$

$$[-O-]_{out} = (2 \times (\langle [NO_2]_{out} \rangle + \langle [CO_2]_{out} \rangle) + \langle [NO]_{out} \rangle + \langle [CO]_{out} \rangle) \frac{FP}{RTm_{C,0}} \tag{28}$$

where P is pressure (1 atm), R is the ideal gas constant, and square brackets denote concentration of gas-phase species in ppm.

Although slight oxidation of carbon with molecular oxygen has been reported at about 400 °C [38], the rate of such a reaction is very low, and in practice, only above 500 °C can significant oxidation rates be observed [82]. This explains the closed balance that was observed for [-O-] in experiments conducted in the presence of molecular oxygen. Only in experiment no. 1 and to a lesser extent in experiment no. 2 could slight differences between the net rates of inflow and outflow of [-O-] be observed. Nevertheless, within those tolerance limits, there is not enough evidence to confirm a previously reported conclusion regarding a noticeable uptake of oxygen from O_2 at 300 and 400 °C [29].

In the presence of water, Jacquot et al. have reported a larger specific rate of oxygen consumption from NO_2 than from the specific rate of oxygen outflow in the reaction products, i.e. NO, CO, and CO_2 [29]. Therefore, a catalytic role has been assumed for water, and the excess of oxygen vanished from the inlet NO_2 has been attributed to the gas-phase formation of HNO_2 and HNO_3. However, the formation of nitric acid in the gas phase is unlikely at the temperature ranges pertinent to carbon oxidation due to the fact that complete dissociation has been reported at $T > 200$ °C [31] (the equilibrium constant for decomposition of nitric acid is in the order of 108 at 350 °C). Furthermore, water was also observed to increase the rate of O_2-based oxidation, which cannot be explained by the formation of nitrous-/nitric acid.

Jeguirim et al. have found that the oxygen balance is closed in the presence of both

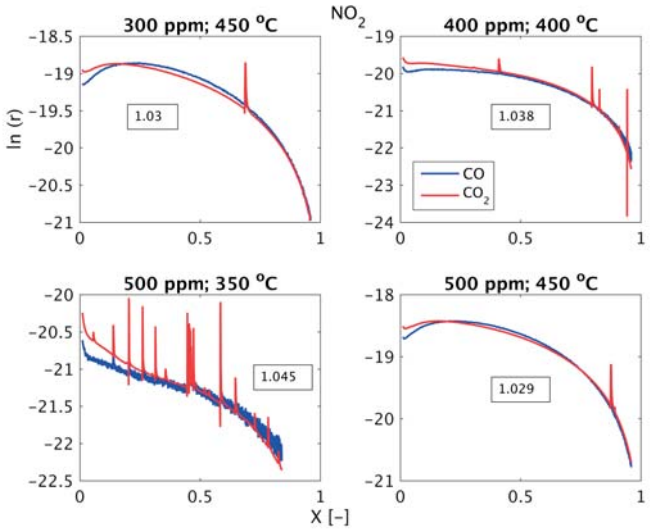

Figure 25: Selectivity as a function of conversion for the C + NO_2 reaction

5% and 10% water [30, 83], and they also considered the promoting effect of water to be of a catalytic type. Similarly, both [-O-] and [-N-] balances were observed to be closed in the study by Messerer et al. [27]. The results presented in Table 3 confirm that both [-O-] and [-N-] balances were closed in all experiments, which indicates a catalytic effect for both water and oxygen at the studied range of temperature. Moreover, the ratio of $[\text{-O-}]_{out}$ to $[\text{-N-}]_{out}$ was, in all experiments, very close to 2:1 (see Table 3), which indicates that the net oxygen transfer was due to NO_2 conversion.

5.5.3 Selectivity

The selectivity of carbon oxidation is in favor of CO with increasing temperature. Figures 25 through 27 show a normalized logarithm of reaction rate profiles of CO and CO_2 versus conversion. In these graphs, the rate of formation of CO_2 has been down-scaled to that of CO using the maxima of the two curves. The number tag in each plot references the multiplier used for scaling. These graphs show that, irrespective of the presence of water and oxygen, the formation of CO and CO_2 varied with conversion in a similar way except at high temperature, and in the early stages of burn-off, CO formation was proportionally higher. This indicates that selectivity is a weak function of conversion.

As noted before (cf. Figure 11), the addition of water mainly enhances the route to

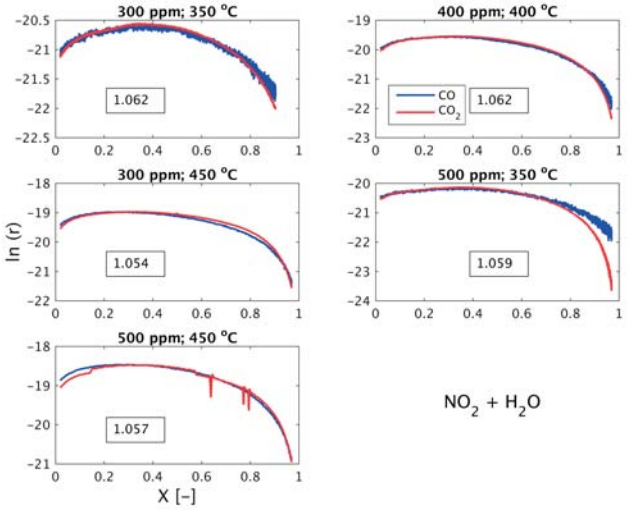

Figure 26: Selectivity as a function of conversion for the C + NO_2 reaction in the presence of water.

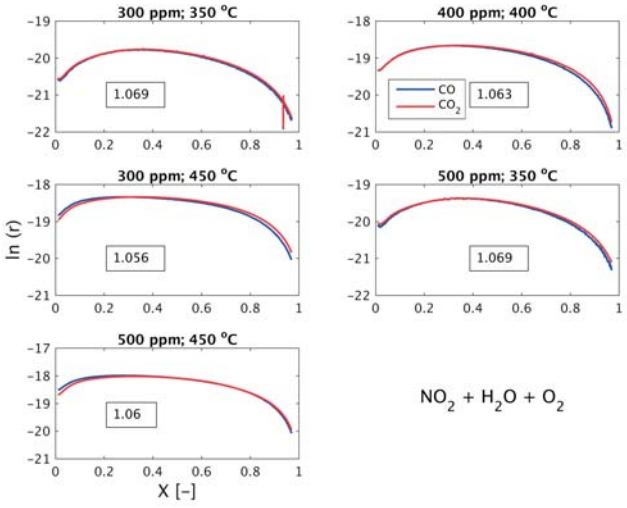

Figure 27: Selectivity as a function of conversion for the C + NO_2 reaction in the presence of water and oxygen.

CO_2 formation [27, 29]. The calculated values for the [CO]:[CO_2] ratio included in Table 3 are within the reported range of 0.2-0.4 [29, 30], and in general, these numbers confirm the effect of water on selectivity. In contrast, the addition of molecular oxygen enhances the formation of both CO and CO_2 (cf. Figure 12). However, CO_2 formation was observed to be more strongly influenced at low temperatures, yet this influence is masked by the effect of temperature on selectivity at $T > 400$ °C (cf. Table 3).

Some studies have found that the water-gas shift reaction can explain the influence of water on selectivity [32, 82]. Nevertheless, the investigated range of temperature in this study and the absence of a catalyst make it unfeasible that the water-gas shift reaction caused the shift in selectivity. A more likely explanation is proposed to be related to the surface oxygen complexes, which will be discussed in the next section.

5.5.4 Effect of surface oxygen complexes

In the presence of NO_2, the chemical structure and thermal stability of surface oxygen complexes that are formed on a carbonaceous surface have been reported in the literature [23, 24]. A study of carbon oxidation in air has also found various types of surface oxygen complexes, and that the desorption of each of those complexes is a function of surface coverage [84].

To scrutinize the interaction between water and surface oxygen complexes, an experiment was conducted in which a degassed sample was exposed to 400 ppm NO_2 at 100 °C. This temperature was chosen to be low enough to prevent oxidation yet high enough to allow for chemisorption. The sample was kept under this condition for about 1 hr to ensure that surface coverage was complete, at which point the outlet concentration of NO_2 was observed to reach the inlet concentration. Next, the gas-phase composition was switched to Ar, 1% water was dosed, and a temperature-programmed desorption (TPD) step was carried out by ramping up the temperature to 650 °C. For the most part of the TPD step, the detected signal of NO_2 was at the baseline level except initially where physically adsorbed NO_2 was observed to desorb for a few minutes. Upon completion of desorption, i.e. when the detected signal of CO and CO_2 dropped to the baseline level, water was removed and the sample was cooled to 100 °C under the flow of argon. The sample was again exposed to 400 ppm NO_2 until the surface coverage was completed as explained above. A second TPD step was carried out, this time in the absence of water,

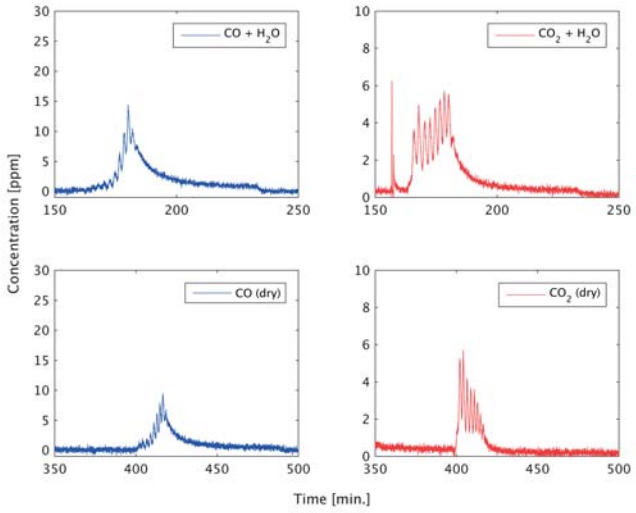

Figure 28: Desorption peaks obtained for CO (left column) and CO_2 (right column) in the presence (top panel) and in the absence of water (bottom panel).

so that the results of the two steps could be compared with one another.

Figure 28 shows the desorption peaks obtained during the two TPD steps for both CO and CO_2. Desorption peaks of both CO and CO_2 showed a distinct increase when water was present during a TPD step, which indicates that water actually interacted with oxygenated complexes on the surface. Integrating the area under the desorption peaks, used as an indication of the total amount of complexes desorbed with time, shows a promoting factor of about 1.8 to 2. It is noteworthy that: i) in both cases, water was not present when oxygen chemisorption took place; and ii) the interaction between water and surface oxygen complexes was examined in the absence of NO_2 in the gas phase. Furthermore, an underlying assumption of this study was that the effect of carbon conversion is negligible between the first and the second TPD steps.

In the research conducted in this thesis, the hypothesis that is put forward is that the presence of water contributes to the formation of carboxylic acid functional groups, which are probably of an anhydride type in the absence of water. Carboxylic acid complexes decompose mainly into CO_2 and H_2O [84], which can explain both the observed shift in selectivity and the catalytic effect (because of the retrieval of a water molecule).

5.5.5 Global kinetic parameters

The kinetics of carbon oxidation, in particular the activation energy and the reaction order of carbon, has been observed to be conversion-dependent (see e.g. Figures 22 through 24 and [34]). The initially negative reaction order of carbon was attributed to increasing porosity and, thus, oxygen access. Therefore, parallel, competing steps are involved that comprise, on the one hand, a gradual increase in porosity and oxygen access, and on the other hand, the removal of active sites with progressive conversion [34, 69]. As discussed in Chapter 4, the random pore model of Bhatia and Perlmutter can be used to model the gradual changes in the porous structure of carbon [40]. The RPM has been regarded as a viable approach for approximating the conversion dependency of the available surface area of carbon [85]. It has been reported to be successful in representing experimental measurements, even though it has not been considered as a fundamental approach for determining the available surface area as a function of conversion [85].

The kinetic model formulated in Section 4.4 can be successfully fitted to the experimental observations with a minimal number of adjustable parameters. The model was fitted to a subset of experiments in which both water and oxygen were present along with NO_2. This was because of the significance of the realistic exhaust conditions to be taken into consideration. The conversion intervals of 0-1%, and 99-100% were not included in the regression analysis. The exclusion of the latter was due to the start of a temperature ramp-up to complete oxidation; nevertheless, Figure 29 shows that the predictions of the model can safely be extrapolated to 100% conversion. The very early phase of the reaction was excluded because of the artifacts that arose from the exposure of the samples to ambient air. Thus quite a different form of kinetics was identified as overshoots in the reaction rate that are restored every time the sample is exposed to air [12]. Nevertheless, such artifacts last for a short period of time, so the model is considered to predict conservative results over the 0-1% conversion interval. This means that the model can cover the entire range of conversion with a very good degree of accuracy.

Table 4 includes the values obtained for the parameters of the kinetic model and their 95% confidence intervals. A fitted structure factor of around 24 indicates that the maximum reaction rate was quickly reached in the presence of both water and oxygen as promoters. The very tight confidence intervals are due to a generally low correlation among the parameters, as shown in Table 5.

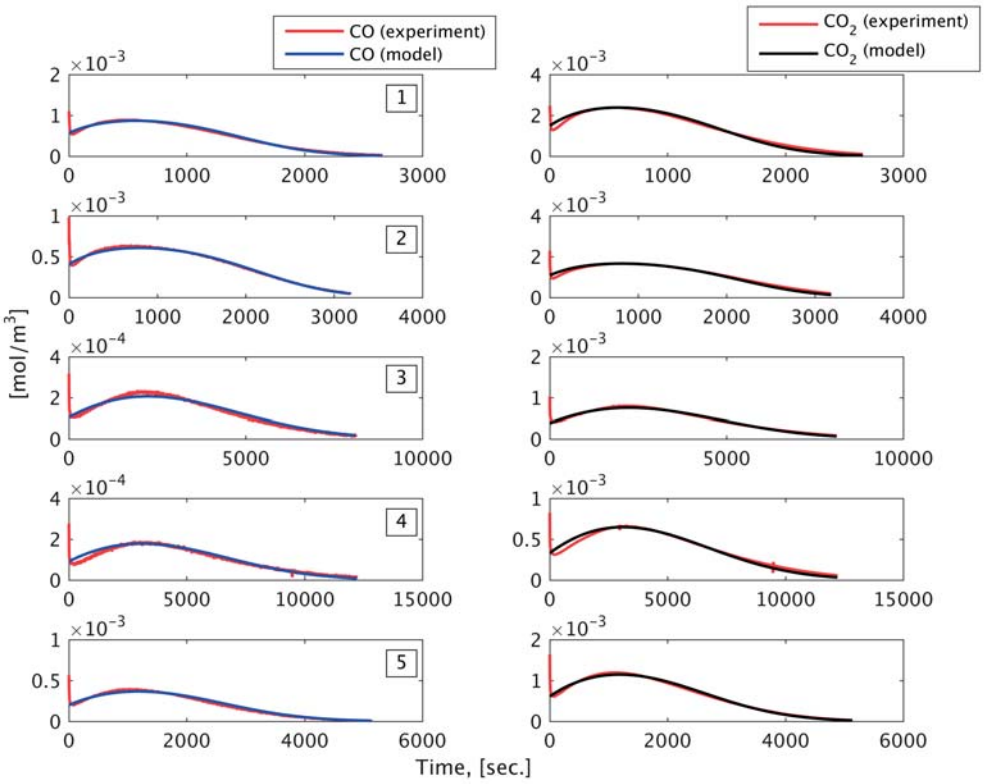

Figure 29: Kinetic model fitted to the experimentally measured concentrations of the oxidation products. The number tag in each plot refers to the corresponding experiment as listed in Table 3.

$A_j \times 10^7[s^{-1}]$	$E\ [\frac{kJ}{mol}]$	$\beta\ [-]$	structure factor [−]
$A_1 = 1.48 \pm 0.03$	$E_1 = 68.2 \pm 0.1$	$\beta_1 = 0.56 \pm 0.00$	$\psi = 24.3 \pm 0.1$
$A_2 = 4.76 \pm 0.03$	$E_2 = 57.7 \pm 0.1$	$\beta_2 = 0.57 \pm 0.00$	

Table 4: Parameters of the kinetic model with their 95% confidence intervals. The pre-exponential values are according to Eq. 7 at a reference temperature of $T_{ref.} = 400$ °C.

A_1	E_1	A_2	E_2	β_1	β_2	ψ
1.0	0.05	0.35	0.20	-0.05	-0.16	-0.52
	1.0	-0.42	-0.26	0.40	-0.61	0.45
		1.0	0.62	-0.42	0.55	-0.87
			1.0	-0.28	0.33	-0.52
				1.0	-0.40	0.66
					1.0	-0.61
						1.0

Table 5: Correlation matrix for the parameters of the kinetic model.

A reaction order of around 0.6 for NO_2 indicates that the adsorption and dissociation of NO_2 on a carbon site is not the rate determining step. This is consistent with the rate of chemisorption being quite fast above 300 °C. It was shown in Section 5.4 that a first-order desorption step cannot fit the experimentally observed rate of decomposition of surface complexes. A similar observation has been made in studies of carbon gasification [62, 63, 64, 86, 87, 88]. This can very well indicate that parallel processes are involved in the formation of CO and CO_2 as the oxidation products. These parallel processes can be speculated to be due to different surface species that are involved in the formation of CO and CO_2, as can be understood from Figure 10 and Table 2. This hypothesis can be strengthened by the outcomes of a temperature-programmed desorption (TPD) study of surface oxygen complexes that has found evidence of the existence of different types of oxygen-containing complexes with different, possibly coverage-dependent, activation energy of desorption [84].

Activation energies that have been reported in the literature span a range of 40-90 kJ/mol [1]. Messerer et al. have proposed a Langmuir-Hinshelwood mechanism with an overall activation energy of 60 to 80 kJ/mol for the adsorption and reaction of NO_2 on four types of carbonaceous matter [27]. For soot oxidation with 500 ppm NO_2 in the presence of 1-5% H_2O, activation energies of about 88 to 144 kJ/mol have been reported

[72]. The fitted activation energies of the model typically coincide with these ranges.

5.6 Design optimization and efficient filter regeneration

Reliable models for simulating soot capture and oxidation along with heat and mass transfer in a soot filter are dependent on the accurate prediction of the kinetics of soot oxidation. Therefore, accurate kinetic models play a crucial role in the optimization of both the design of particulate filters and the operation of diesel engines. The efficient regeneration of DPFs requires predicting the extent to which passive regeneration can be relied on and the required temperature and concentration of NO_2 in diesel exhaust to achieve a balance-point between the rate of soot oxidation and that of soot deposition [34]. Thus the frequency of active regeneration cycles can be adjusted to minimize fuel penalty and the risk of melting the filter due to an uncontrolled regeneration.

Using the algorithm proposed in Section 4.6, Eq. 12 was integrated to estimate the exhaust conditions required to maintain the engine back pressure within the required limits. For a light-duty engine, a maximum pressure-drop of approx. 100 mbar can be allowed [85]. This would correspond to an accumulated soot of about 10 g/l, neglecting ash formation in aged traps [89]. For a 2-liter filter ($\Phi = 5.66$ in., $L = 5$ in.), a total soot-mass loading of 20 g is deduced. As shown in Figure 30, for an uncoated filter to achieve that limit at as low a temperature as 300 °C would demand an upstream diesel oxidation catalyst to produce about 900 ppm NO_2.

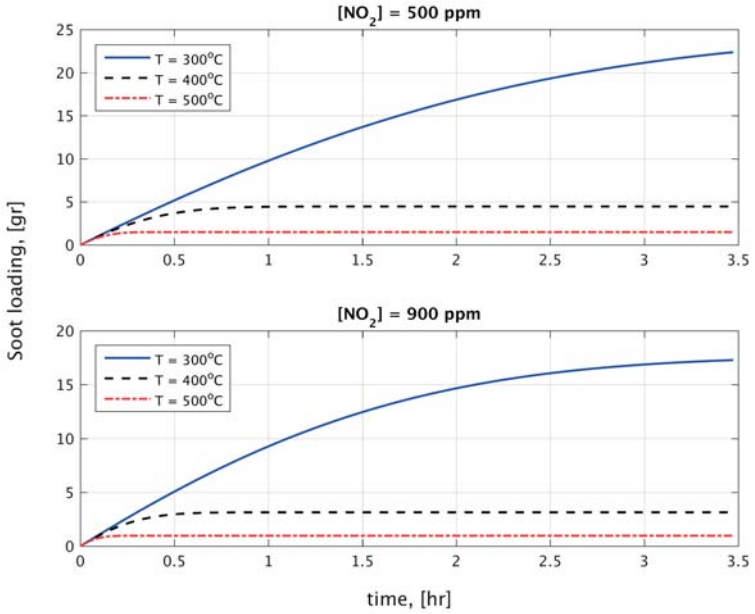

Figure 30: Results of simulating the kinetic model used to predict the temperature and NO_2 concentration in diesel exhaust required to reach steady-state conditions in a soot trap.

6

Conclusions and Outlook

The goal of this research was primarily to develop experimental and theoretical methodologies for studying diesel soot oxidation in diesel particulate filters. An additional aim was to investigate the promoting effect of water and oxygen, which are abundant species in diesel exhaust.

To fulfill these goals, a thorough characterization study of the reactor setup was conducted with a prime focus on heat transfer and residence time distribution. Using computational fluid dynamics simulations, it was found that radiative heat transfer is an important mechanism of heat transfer at elevated temperatures, and, therefore, shielding the sample from radiation is crucial to minimize temperature gradients along the monolithic reactor. In addition to this, **Paper II** includes a number of guidelines that were found to be helpful for improving the quality of experimental measurements, in particular temperature distributions over the sample.

The analysis of residence time distribution in **Paper II** identified the contribution of various parts of the experimental setup to the overall loss of temporal resolution in transient experiments. It also showed that IR-based spectroscopy of species with non-linear IR absorption is prone to a systematic error in transient experiments if a non-uniform concentration distribution prevails in the gas cell of the detector. This was proven in **Paper IV**, and the error was quantified for CO and NO, i.e. two species with known non-linear IR absorption, by developing a CFD model for a gas cell. It was proposed that a compartment model for the gas cell be used to circumvent the error.

A deconvolution algorithm was developed to decrease the unresolved time interval in

transient experiments. The algorithm uses the Tikhonov regularization method to address the ill-posed, inverse problem of deconvolution. The algorithm was described in detail in **Paper III**, and it was shown to be successful in handling experimental noise in the measured data. The algorithm was released as an Open Source package and has since found users at other institutions. A deconvolution algorithm is also useful to uncouple the contribution of individual, consecutive regions of a flow system with respect to residence time distribution in the overall system. This was helpful for the analysis of transient measurements relating to carbon oxidation using step-response experiments. An important achievement of that study was the evidence found for the existence of parallel mechanisms and also the possibility of having more than one surface species involved in the formation of the oxidation products, i.e. CO and CO_2. Likewise, in a collaborative study with the Catalysis Engineering group at Delft University of Technology, the algorithm was used to characterize residence time distribution in different parts of a multiphase, tubular reactor with structured packings.

The study of this thesis found experimental evidence of the promoting effect of water and oxygen for the C + NO_2 reaction. Furthermore, a synergistic effect was observed when water, oxygen, and NO_2 were simultaneously present in the gas phase. This signifies the importance of taking realistic exhaust conditions into consideration. **Paper V** includes the results of a kinetic study of carbon oxidation with NO_2 in the presence of water and oxygen. It was found that the reaction order of carbon is strongly dependent on the degree of conversion, while the selectivity of the reaction is a weak function of conversion. Evaluating the [-O-] and [-N-] balance showed that the net oxygen transfer with respect to the formation of the oxidation products, i.e. NO, CO, and CO_2, can be explained with NO_2 conversion. In other words, within the temperature window chosen for the present study, neither molecular oxygen nor water participates in oxygen transfer on a net basis. Subsequently, a global kinetic model was developed that was successfully fitted to the experimentally measured rate of carbon oxidation at various temperatures and inlet concentrations of NO_2. The model can be used for the entire conversion interval with a very good degree of accuracy.

Of central importance for the experimental study of the present research was improvement to the previous method of sample preparation that was based on shaking a monolithic substrate together with the dry powder of soot in a container. It was found that samples prepared using the previous method were susceptible to non-uniform carbon

deposition among and within the channels of the substrate. This study proposed to use a thin brush, instead, for coating the interior walls of the substrate with carbon, thereby achieving much better control over the carbon deposition in each and every channel. The results obtained with this method showed a high degree of consistency and reproducibility.

Conversion dependency of the reaction order of carbon was approximated using a random pore model. The random pore model is a mathematical model that derives a theoretical expression for the available surface area of carbon as a function of conversion. The fact that the observed reaction rate is a function of conversion implies that the age distribution of carbon in a soot filter has a significant impact on the reactivity of the soot cake towards oxidation. Therefore, in **Papers I** and **V**, a simplified population balance model was formulated to keep track of conversion in a soot filter. An algorithm was formulated for solving the population balance model that relies on the assumption of constant temperature and concentration of NO_2, which is a restrictive assumption with respect to the temperature and concentration gradients that typically exist during the regeneration of a soot trap.

Consequently, the research of this thesis can be continued by developing a CFD model for a soot filter that can resolve such temperature and concentration gradients along with the kinetics of carbon oxidation. The global kinetic model developed in this study can easily be integrated with that model. On the other hand, obtaining the kinetics of real PM is of great interest despite the fact that the reactivity of diesel soot differs appreciably depending on the origin of the soot and the driving cycles under which it is collected. Furthermore, formulating a detailed kinetic model can be useful for gaining insight into the mechanistic aspects of carbon oxidation. In particular, using surface analysis techniques, such as DRIFTS, can aid in understanding the details and shedding light on the mechanisms through which water and oxygen enhance the oxidation reaction. Such information seems to be missing in the current body of literature published on this subject.

Nomenclature

A	pre-exponential factor [unit depends on the reaction rate equation]
C_f	free carbon site on the edge plane
C_b	a carbon atom on the basal plane
$C(O)$	oxygen-complexes on the edge plane
$C_b(O)C(O)$	the proposed complex consisting of an oxygen atom bonded to a carbon atom on the basal plane which is adjacent to a an already oxygenated carbon site on the edge plane
E	activation energy [J/mol]
$E(t)$	residence time distribution [s^{-1}]
f	solid-state decomposition model
F	volumetric flow rate [m^3/s]
g	transfer function [arb. u.]
h	function of concentration representing concentration dependency of the reaction rate [arb. u.]
k	rate constant [unit depends on the reaction rate equation]
L	length, [m]
$\dot{m}$	mass flow rate [kg/s]
m	mass [kg]
MW	molecular weight [gr/mol]

N	active site density $[mol/m^2]$
p_i	partial pressure of species i [Pa]
P	pressure [Pa]
r	rate of carbon oxidation $[\frac{mol}{gr_C.\mathrm{s}}]$
R	ideal gas constant $[\frac{J}{mol.K}]$
S_a	specific surface area $[\frac{m^2}{gr_C}]$
t	time [s]
T	temperature [K]
V	volume $[m^3]$
x	undistorted signal [arb. u.]
X	conversion [-]
y	measured signal [arb. u.]

Greek letters

β	reaction order [-]
η	efficiency [-]
Φ	diameter [m]
ψ	structure factor

Subscripts

0	initial
C	carbon
i	tank index in the tanks-in-series model
$ref.$	reference
t	related to a tank in the tanks-in-series model

Acknowledgements

I would like to express my greatest and deepest gratitude to my supervisors, Prof. Bengt Andersson and Docent Ronnie Andersson for giving me the opportunity to pursue my graduate studies within your research group, for all your help and encouragement when it was most needed, and for our inspiring discussions.

The Competence Centre for Catalysis, which is hosted by Chalmers University of Technology and financially supported by the Swedish Energy Agency and the member companies: AB Volvo, ECAPS AB, Haldor Topsøe A/S, Scania CV AB, Volvo Car Corporation AB and Wärtsilä Finland Oy, are gratefully acknowledged for financially supporting this project.

My sincere thanks are due to all my present and former colleagues and friends at KAT/KRT and KCK. It has always been a great pleasure to share this journey with you. I would especially like to thank Malin Larsson, Mattias Zetterberg and all my colleagues who took the time to help me when things went wrong in the lab.

Special thanks go to Houman, Jon Kristensen, Masoud, Oana, Olle, and Rojin for all the fantastic times I have had with you along the way. I am grateful to Maulana and Mohsen with whom I have shared an office and also had lots of great time playing volleyball and having nice conversations.

And last but foremost, my mother, Goli, and my sister, Mojan, for all your love, support, and care. You are the most valuable part of my life.

Soheil Soltani

Gothenburg, 2017

References

[1] B. R. Stanmore, V. Tschamber, and J. F. Brilhac. **Oxidation of carbon by NOx, with particular reference to NO2 and N2O**. *Fuel*, **87**(2):131–146, 2008. 1, 5, 19, 51

[2] **IARC: diesel engine exhaust carcinogenic**. *Cent Eur J Public Health*, **20**(2):120–138, 2012. 1

[3] Herbert J Tobias, Derek E Beving, Paul J Ziemann, Hiromu Sakurai, Miriam Zuk, Peter H McMurry, Darrick Zarling, Robert Waytulonis, and David B Kittelson. **Chemical Analysis of Diesel Engine Nanoparticles Using a Nano-DMA/Thermal Desorption Particle Beam Mass Spectrometer**. *Environmental Science & Technology*, **35**(11):2233–2243, jun 2001. 1, 2

[4] Robert D Brook, Sanjay Rajagopalan, C Arden Pope, Jeffrey R Brook, Aruni Bhatnagar, Ana V Diez-Roux, Fernando Holguin, Yuling Hong, Russell V Luepker, Murray A Mittleman, Annette Peters, David Siscovick, Sidney C Smith, Laurie Whitsel, Joel D Kaufman, on behalf of the American Heart Association Council on Epidemiology, Council on the Kidney in Cardiovascular Disease Prevention, Physical Activity Council on Nutrition, and Metabolism. **Particulate Matter Air Pollution and Cardiovascular Disease: An Update to the Scientific Statement From the American Heart Association**. *Circulation*, **121**(21):2331–2378, 2010. 1

[5] Susan C Anenberg, Larry W Horowitz, Daniel Q Tong, and J Jason West. **An estimate of the global burden of anthropogenic ozone and fine particulate matter on premature human mortality using atmospheric modeling.** *Environmental health perspectives*, **118**(9):1189–1195, sep 2010. 1

[6] Michael D Hays and Randy L Vander Wal. **Heterogeneous Soot Nanostructure in Atmospheric and Combustion Source Aerosols**. *Energy & Fuels*, **21**(2):801–811, mar 2007. 2

[7] L. R. Radovic. **Active Sites in Graphene and the Mechanism of CO2 Formation in Carbon Oxidation**. *Journal of the American Chemical Society*, **131**(47):17166–17175, 2009. 3

[8] Ljubisa R. Radovic, Alejandro B. Silva-Tapia, and Fernando Vallejos-Burgos. **Oxygen migration on the graphene surface. 1. Origin of epoxide groups**. *Carbon*, **49**(13):4218–4225, 2011. 3

[9] Ljubisa R. Radovic, Alejandro Suarez, Fernando Vallejos-Burgos, and Jorge O. Sofo. **Oxygen migration on the graphene surface. 2. Thermochemistry of basal-plane diffusion (hopping)**. *Carbon*, **49**(13):4226–4238, 2011. 3

[10] Randy L. Vander Wal, Aleksey Yezerets, Neal W. Currier, Do Heui Kim, and Chong Min Wang. **HRTEM Study**

of diesel soot collected from diesel particulate filters. *Carbon*, **45**(1):70–77, 2007. 3, 4, 5

[11] Soheil Soltani, Carolin Wang-Hansen, Ronnie Andersson, and Bengt Andersson. **CFD characterization of monolithic reactors for kinetic studies**. *The Canadian Journal of Chemical Engineering*, **92**(9):1570–1578, 2014. 7, 13, 16, 25, 31, 32, 33, 34, 35

[12] C. Wang-Hansen, C. J. Kamp, M. Skoglundh, B. Andersson, and P. A. Carlsson. **Experimental Method for Kinetic Studies of Gas-Solid Reactions: Oxidation of Carbonaceous Matter**. *Journal of Physical Chemistry C*, **115**(32):16098–16108, 2011. 8, 14, 49

[13] M. F. Modest. **The Method of Discrete Ordinates**. In *Radiative Heat Transfer*, page 498. Academic Press, Amsterdam, 2nd editio edition, 2003. 14

[14] **https://github.com/soheil-soltani/TranKin**. 14

[15] Soheil Soltani, Ronnie Andersson, and Bengt Andersson. **Time Resolution in Transient Kinetics**. In Larisa Beilina, editor, *Inverse Problems and Applications*, pages 81–96. Springer International Publishing, Cham, 2015. 14, 34

[16] C. W. Groetsch. *The Theory of Tikhonov Regularization for Fredholm Equations of the First Kind*. Pitman Advanced Pub. Program, 1984. 15

[17] Jacques Hadamard. **Sur les problèmes aux dérivés partielles et leur signification physique**. *Princeton University Bulletin*, **13**:49–52, 1902. 15

[18] P. C. Hansen and D. P. Oleary. **The Use of the L-Curve in the Regularization of Discrete ilI-Posed Problems**. *Siam Journal on Scientific Computing*, **14**(6):1487–1503, 1993. 15

[19] A. N. Tikhonov and V. Y. Arsenin. *Solutions of Ill-posed Problems*. Winston and Sons, Washington, D.C., 1977. 15

[20] V. A. Morozov. **The error principle in the solution of operational equations by the regularization method**. *USSR Computational Mathematics and Mathematical Physics*, **8**(2):63–87, 1968. 15

[21] C. R. Vogel. **Non-convergence of the L-curve regularization parameter selection method**. *Inverse Problems*, **12**(4):535–547, 1996. 15

[22] Soheil Soltani, Ronnie Andersson, and Bengt Andersson. **Enhancement of time resolution in transient kinetics**. *Chemical Engineering Journal*, **264**:188–196, 2015. 16, 35

[23] Harald Muckenhuber and Hinrich Grothe. **A DRIFTS study of the heterogeneous reaction of NO2 with carbonaceous materials at elevated temperature**. *Carbon*, **45**(2):321–329, 2007. 17, 18, 47

[24] Harald Muckenhuber and Hinrich Grothe. **The heterogeneous reaction between soot and NO2 at elevated temperature**. *Carbon*, **44**(3):546–559, 2006. 18, 19, 20, 47

[25] H. Marsh and A. D. Foord. **Mechanisms of Oxidation of Carbon by Molecular-Oxygen**. *Carbon*, **11**(4):421–424, 1973. 19

[26] Harry Marsh and Francisco Rodríguez-Reinoso. **Chapter 5 - Activation Processes (Thermal or Physical)**. In Harry Marsh and Francisco Rodríguez-Reinoso, editors, *Activated Carbon*, pages 243–321. Elsevier Science Ltd, Oxford, 2006. 19, 38

[27] A. Messerer, R. Niessner, and U. Pöschl. **Comprehensive kinetic characterization of the oxidation and gasification of model and real diesel soot by nitrogen oxides and oxygen under engine exhaust conditions: Measurement, Langmuir-Hinshelwood, and Arrhenius parameters**. *Carbon*, **44**(2):307–324, 2006. 19, 20, 45, 47, 51

[28] M. Jeguirim, V. Tschamber, J. F. Brilhac, and P. Ehrburger. **Interaction mechanism of NO2 with carbon black: Effect of surface oxygen complexes**. *Journal of Analytical and Applied Pyrolysis*, **72**(2):171–181, 2004. 19

[29] F. Jacquot, V. Logie, J. F. Brilhac, and P. Gilot. **Kinetics of the oxidation of carbon black by NO2 influence of the presence of water and oxygen**. *Carbon*, **40**(3):335–343, 2002. 19, 20, 44, 47

[30] M. Jeguirim, V. Tschamber, and J. F. Brilhac. **Kinetics and mechanism of the oxidation of carbon by NO2 in the presence of water vapor**. *International Journal of Chemical Kinetics*, **41**(4):236–244, 2009. 19, 45, 47

[31] W. R. Ellis and R. C. Murray. **The thermal decomposition of anhydrous nitric acid vapour**. *Journal of Applied Chemistry*, **3**(7):318–322, may 2007. 20, 44

[32] A. Fredrik Ahlström and C. U. Ingemar Odenbrand. **Combustion characteristics of soot deposits from diesel engines**. *Carbon*, **27**(3):475–483, 1989. 20, 47

[33] Nabila Zouaoui, Madona Labaki, and Mejdi Jeguirim. **Diesel soot oxidation by nitrogen dioxide, oxygen and water under engine exhaust conditions: Kinetics data related to the reaction mechanism**. *Comptes Rendus Chimie*, **17**(7):672–680, 2014. 21

[34] C. Wang-Hansen, S. Soltani, and B. Andersson. **Kinetic Analysis of O2- and NO2-Based Oxidation of Synthetic Soot**. *The Journal of Physical Chemistry C*, **117**(1):522–531, jan 2013. 22, 25, 26, 28, 49, 52

[35] Aleksey Yezerets, Neal W Currier, and Heather A Eadler. **Experimental Determination of the Kinetics of Diesel Soot Oxidation by O2 - Modeling Consequences**, 2003. 23

[36] P. Darcy, P. Da Costa, H. Mellottee, J. M. Trichard, and G. Djega-Mariadassou. **Kinetics of catalyzed and non-catalyzed oxidation of soot from a diesel engine**. *Catalysis Today*, **119**(1-4):252–256, 2007. 23

[37] A. Yezerets, N. W. Currier, D. H. Kim, H. A. Eadler, W. S. Epling, and C. H. F. Peden. **Differential kinetic analysis of diesel particulate matter (soot) oxidation by oxygen using a step-response technique**. *Applied Catalysis B-Environmental*, **61**(1-2):120–129, 2005. 23

[38] Guido Mul. *Catalytic diesel exhaust purification.* PhD thesis, Delft University of Technology, Delft, 1997. 23, 44

[39] F. Kapteijn and J. A. Moulijn. **Kinetics of Catalysed and Uncatalysed Coal Gasification**. In Jose L Figueiredo and Jacob A Moulijn, editors, *Carbon and Coal Gasification: Science and Technology*, **105**, pages 291–360. Springer, Netherlands, Dordrecht, 1986. 23, 24

[40] S. K. Bhatia and D. D. Perlmutter. **A random pore model for fluid-solid reactions: I. Isothermal, kinetic control**. *AIChE Journal*, **26**(3):379–386, may 1980. 23, 26, 49

[41] George R. Gavals. **A random capillary model with application to char gasification at chemically controlled rates**. *AIChE Journal*, **26**(4):577–585, jul 1980. 23

[42] Sebastián Reyes and Klavs F. Jensen. **Percolation concepts in modelling of gas-solid reactions–I. Application to char gasification in the kinetic regime**. *Chemical Engineering Science*, **41**(2):333–343, 1986. 23

[43] Muhammad Sahimi. *Applications of percolation theory*. Taylor & Francis, London, 1994. 23

[44] F. Kapteijn, R. Meijer, J. A. Moulijn, and D. Cazorlaamoros. **On Why Do Different Carbons Show Different Gasification Rates - a Transient Isotopic CO2 Gasification Study**. *Carbon*, **32**(7):1223–1231, 1994. 24, 25, 38

[45] H. Jiang and L. R. Radovic. **Transient Kinetic-Studies of Char Gasification in Carbon-Dioxide**. *Abstracts of Papers of the American Chemical Society*, **197**:36–Fuel, 1989. 24, 25

[46] P. Ehrburger, F. Louys, and J. Lahaye. **The concept of active sites applied to the study of carbon reactivity**. *Carbon*, **27**(3):389–393, 1989. 24

[47] W.P. Huffman. **The importance of active surface area in the heterogeneous reactions of carbon**. *Carbon*, **29**(6):769–776, 1991. 24

[48] N. R. Laine, F. J. Vastola, and P. L. Walker. **Importance of Active Surface Area in Carbon-Oxygen Reaction**. *Journal of Physical Chemistry*, **67**(10):2030–&, 1963. 24

[49] T. Nozaki, T. Adschiri, and T. Furusawa. **Characterization of Coal Char Reactivity by Transient Kinetics Technique**. *Fuel Processing Technology*, **24**:277–283, 1990. 24, 25

[50] Rob J. Berger, Freek Kapteijn, Jacob A. Moulijn, Guy B. Marin, Juray De Wilde, Maria Olea, De Chen, Anders Holmen, Luca Lietti, Enrico Tronconi, and Yves Schuurman. **Dynamic methods for catalytic kinetics**. *Applied Catalysis A: General*, **342**(1-2):3–28, 2008. 24, 25

[51] D. Y. Murzin and T. Salmi. **Chapter 8 - Dynamic Catalysis**. In *Catalytic Kinetics*, pages 285–339. Elsevier Science, 2005. 25

[52] E. Muller and H. Hofmann. **Dynamic Modeling of Heterogeneous Catalytic Reactions .2. Experimental Results - Oxydehydrogenation of Isobutyric Aldehyde to Methacrolein**. *Chemical Engineering Science*, **42**(7):1705–1715, 1987. 25

[53] F. Kapteijn, R. Meijer, and J. A. Moulijn. **Transient Kinetic Techniques**

for Detailed Insight in Gas Solid Reactions. *Energy & Fuels*, **6**(4):494–497, 1992. 25

[54] Carroll O Bennett. **The Transient Method and Elementary Steps in Heterogeneous Catalysis**. *Catalysis Reviews*, **13**(1):121–148, jan 1976. 25

[55] Haruo Kobayashi and Masayoshikobayashi. **Transient Response Method in Heterogeneous Catalysis**. *Catalysis Reviews*, **10**(1):139–176, jan 1974. 25

[56] Masayoshi Kobayashi. **Characterization of transient response curves in heterogeneous catalysis–I. Classification of the curves**. *Chemical Engineering Science*, **37**(3):393–401, 1982. 25

[57] E. Muller and H. Hofmann. **Dynamic Modeling of Heterogeneous Catalytic Reactions .1. Theoretical Considerations**. *Chemical Engineering Science*, **42**(7):1695–1704, 1987. 25

[58] T. Salmi. **Modeling and Simulation of Transient States of Ideal Heterogeneous Catalytic Reactors**. *Chemical Engineering Science*, **43**(3):503–511, 1988. 25

[59] P. Biloen. **Transient Kinetic Methods**. *Journal of Molecular Catalysis*, **21**(Oct):17–24, 1983. 25

[60] M. B. Cutlip, C. C. Yang, and C. O. Bennett. **Parameter Estimation from Transient Rate Data**. *Aiche Journal*, **18**(5):1073–&, 1972. 25

[61] F. Bonner and J. Turkevich. **Study of the Carbon Dioxide Carbon Reaction Using C-14 as a Tracer**. *Journal of the American Chemical Society*, **73**(2):561–564, 1951. 25

[62] F. Kapteijn, R. Meijer, and J. A. Moulijn. **A Transient Kinetic Study of the Gasification of Carbon in CO2**. *Abstracts of Papers of the American Chemical Society*, **202**:906–913l, 1991. 25, 51

[63] T. Adschiri, T. Nozaki, T. Furusawa, and Z. B. Zhu. **Characterization of Coal Char Gasification Rate**. *Aiche Journal*, **37**(6):897–904, 1991. 25, 51

[64] H Freund. **Gasification of Carbon by CO2 - A Transient Kinetics Experiment**. *Fuel*, **65**(1):63–66, 1986. 25, 51

[65] T. M. Crick, P. L. Silveston, K. Miura, and K. Hashimoto. **Analysis of Coal Char Gasification by Use of the Pulse Method and O-18 Isotope**. *Energy & Fuels*, **7**(6):1054–1061, 1993. 25

[66] F. J. Vastola, P. J. Hart, and P. L. Walker. **A Study of Carbon Oxygen Surface Complexes Using O-18 as a Tracer**. *Carbon*, **2**(1):65–71, 1964. 25

[67] Melvin Avrami. **Kinetics of Phase Change. I General Theory**. *The Journal of Chemical Physics*, **7**(12), 1939. 26

[68] Ammar Khawam and Douglas R. Flanagan. **Solid-state kinetic models: Basics and mathematical fundamentals**. *Journal of Physical Chemistry B*, **110**(35):17315–17328, 2006. 26

[69] S. V. Vyazovkin and A. I. Lesnikovich. **On the method of solving the inverse problem of solid-phase reaction kinetics**. *Journal of thermal analysis*, **36**(2):599–615, 1990. 26, 49

[70] Chethan K. Gaddam, Randy L. Vander Wal, Xu Chen, Aleksey Yezerets, and Krishna Kamasamudram. **Reconciliation of carbon oxidation rates and activation energies based on changing nanostructure**. *Carbon*, **98**:545–556, 2016. 26

[71] K. Otto, M. H. Sieg, M. Zinbo, and L. Bartosiewicz. **The oxidation of soot deposits from diesel engines**, 1980. 26

[72] Jens Oliver Müller, Benjamin Frank, Rolf E Jentoft, Robert Schlögl, and Dang Sheng Su. **The oxidation of soot particulate in the presence of NO2**. *Catalysis Today*, **191**(1):106–111, 2012. 26, 52

[73] H.S. Fogler. **Models for nonideal reactors**. In *Elements of Chemical Reaction Engineering*, chapter 14, page pp. 948. Prentice Hall, New Jersey, 2006. 27

[74] Jung W Suh and Youngmin Kim. *Accelerating MATLAB with GPU computing: a primer with examples*. Elsevier, Amsterdam, 1st edition, 2014. 30

[75] Björn Lundberg. *Aspects of efficient parameter estimation for diesel oxidation catalysts*. PhD thesis, Chalmers University of Technology, 2015. 30

[76] O. Levenspiel. *Chemical Reaction Engineering*. John Wiley & Sons Inc., New York, 3rd editio edition, 1999. 33

[77] R. Aris. **On The Dispersion of a Solute in a Fluid Flowing Through a Tube**. *Proceedings of the Royal Society of London Series a-Mathematical and Physical Sciences*, **235**(1200):67–77, 1956. 34

[78] Geoffrey Taylor. **Dispersion of Soluble Matter in Solvent Flowing Slowly through a Tube**. *Proceedings of the Royal Society of London. Series A. Mathematical and Physical Sciences*, **219**(1137):186–203, 1953. 34

[79] Axel Olsson. *A modeling framework for resolving non-linear infrared absorbation in an FTIR cell*. Master's thesis, Chalmers University of Technology, 2015. 37

[80] P. L. Walker Jr, F. J. Vastola, and P. J. Hart. **Oxygen-18 Tracer Studies on the Carbon-Oxygen Reaction**. In Howard Saltsburg and Joe N Smithmilton Rogers, editors, *Fundamentals of Gas–Surface Interactions*, pages 307–317. Academic Press, 1967. 38

[81] W. H. Press, S. A. Teukolsky, W. T. Vetterling, and B. P. Flannery. **Statistical Description of Data**. In *Numerical Recipes*, chapter 14, page 644. Cambridge University Press, New York, 3rd edition, 2007. 42

[82] J. P. A. Neeft, T. X. Nijhuis, E. Smakman, M. Makkee, J. A. Moulijn. **Kinetics of the oxidation of diesel soot**. *Fuel*, **76**(12):1129–1136, oct 1997. 44, 47

[83] M. Jeguirim, V. Tschamber, J. F. Brilhac, and P. Ehrburger. **Oxidation mechanism of carbon black by NO2: Effect of water vapour**. *Fuel*, **84**(14-15):1949–1956, 2005. 45

[84] G. Tremblay, F. J. Vastola, and P. L. Walker. **Thermal desorption analysis of oxygen surface complexes on carbon**. *Carbon*, **16**(1):35–39, 1978. 47, 48, 51

[85] Barry A A L van Setten, Michiel Makkee, and Jacob A Moulijn. **Science and**

technology of catalytic diesel particulate filters. *Catalysis Reviews*, **43**(4):489–564, 2001. 49, 52

[86] K. J. Huttinger and J. S. Nill. **A Method for the Determination of Active-Sites and True Activation-Energies in Carbon Gasification .2. Experimental Results**. *Carbon*, **28**(4):457–465, 1990. 51

[87] A. A. Lizzio, H. Jiang, and L. R. Radovic. **On the Kinetics of Carbon (Char) Gasification - Reconciling Models with Experiments**. *Carbon*, **28**(1):7–19, 1990. 51

[88] L. R. Radovic, H. Jiang, and A. A. Lizzio. **A Transient Kinetics Study of Char Gasification in Carbon-Dioxide and Oxygen**. *Energy & Fuels*, **5**(1):68–74, 1991. 51

[89] Alexander Sappok and Victor W Wong. **Lubricant-Derived Ash Properties and Their Effects on Diesel Particulate Filter Pressure-Drop Performance**. *Journal of Engineering for Gas Turbines and Power-Transactions of the ASME*, **133**(3), mar 2011. 52